

1 **Influence of the convection electric field models on predicted**  
2 **plasmopause positions during magnetic storms**

3  
4 Pierrard V.<sup>1,3</sup>, G. Khazanov<sup>2</sup>, J. Cabrera<sup>3</sup> and J. Lemaire<sup>1,3</sup>

5  
6 1 Belgian Institute for Space Aeronomy, 3 av. Circulaire, B-1180 Brussels, Belgium  
7 Tel: (32 2)3730418, Fax: (32 2)3748423, email: viviane.pierrard@oma.be

8  
9 2 National Space Science and Technology Center, NASA Marshall Space Flight Center,  
10 Huntsville, Alabama 35899, USA

11  
12 3 Center for Space Radiations, UCL, 2 chemin du cyclotron, 1348 Louvain-La-Neuve,  
13 Belgium

14  
15 **Abstract:**

16 In the present work, we determine how three well documented models of the  
17 magnetospheric electric field, and two different mechanisms proposed for the formation  
18 of the plasmopause influence the radial distance, the shape and the evolution of the  
19 plasmopause during the geomagnetic storms of 28 October 2001 and of 17 April 2002.  
20 The convection electric field models considered are: McIlwain's E5D electric field  
21 model, Volland-Stern's model and Weimer's statistical model compiled from low-Earth  
22 orbit satellite data. The mechanisms for the formation of the plasmopause to be tested are:  
23 (i) the MHD theory where the plasmopause should correspond to the last-closed-  
24 equipotential (LCE) or last-closed-streamline (LCS), if the E-field distribution is  
25 stationary or time-dependent respectively; (ii) the interchange mechanism where the  
26 plasmopause corresponds to streamlines tangent to a Zero-Parallel-Force surface where  
27 the field-aligned plasma distribution becomes convectively unstable during enhancements  
28 of the E-field intensity in the nightside local time sector.

29 The results of the different time dependent simulations are compared with concomitant  
30 EUV observations when available. The plasmatails or plumes observed after both  
31 selected geomagnetic storms are predicted in all simulations and for all E-field models.  
32 However, their shapes are quite different depending on the E-field models and the  
33 mechanisms that are used. Despite the partial success of the simulations to reproduce  
34 plumes during magnetic storms and substorms, there remains a long way to go before the  
35 detailed structures observed in the EUV observations during periods of geomagnetic  
36 activity can be accounted for very precisely by the existing E-field models. Furthermore,  
37 it cannot be excluded that the mechanisms currently identified to explain the formation of  
38 "Carpenter's knee" during substorm events, will have to be revised or complemented in  
39 the cases of geomagnetic storms.

40  
41  
42 **1. Introduction.**

43  
44 The plasmopause position prediction is very important for the scientific community  
45 because its location determines the influence of wave-particle interaction processes on

1 radiation belts (RB) formation. Cornwall et al. [1971] noted that maximum instability of  
2 ElectroMagnetic Ion Cyclotron (EMIC) waves generated by ring current (RC) anisotropy  
3 should occur just within the plasmopause. He also suggested that pitch-angle diffusion of  
4 RC ions resonant with the EMIC waves generated within the plasmopause should be  
5 important loss process for the RC. Recent global self-consistent RC/EMIC waves  
6 modeling by Khazanov et al. [2006] conforms this initial study. It was found that global  
7 EMIC wave distribution has a highly plasmopause organized structure during the May,  
8 1998 storm period that has been presented in this study. Khazanov et al. [2007] also  
9 found that plasmaspheric energy deposition to the thermal electrons via Landau EMIC  
10 wave damping is very critical to position of plasmopause.

11

12 During magnetic storms, under certain conditions, relativistic electrons with energies  $\geq 1$   
13 MeV can be removed from the outer RB by EMIC wave scattering. Recent calculations  
14 suggest that pitch angle scattering via EMIC waves can compete with  $D_{st}$  effect as a  
15 mechanism for depleting relativistic electrons from the outer RB zone during the initial  
16 and main phases of a magnetic storm [Summers and Thorne, 2003; Albert, 2003]. So, it  
17 becomes more and more obvious that RC and RB populations are very sensitive to the  
18 core plasmasphere distribution and specifically to the position of the plasmopause  
19 [Spasojevic et al., 2004; Baker et al., 2004].

20

21 The position of the plasmopause is determined by the interplay between the co-rotation  
22 and convection electric fields. This statement is very general but it does not really  
23 identify and grasp the specific physical mechanism that is underlying the formation of the  
24 plasmopause. The magnetospheric convection electric field, controlled by the solar wind  
25 conditions and the level of geomagnetic activity, is a key factor in all existing theories for  
26 the formation of the plasmopause. Therefore, it is important to have first a reliable  
27 magnetospheric electric field model. Since there is no way to determine directly, at each  
28 instant of time, the global electric field distribution in the whole magnetosphere, various  
29 empirical and mathematical models have been built, tentatively, with various degrees of  
30 sophistication. The E-field models used in the present paper are (i) the VSMC model  
31 introduced by Volland and Stern [Volland, 1973; Stern, 1975] and adapted by Maynard

1 and Chen [1975], (ii) the E5D model derived by McIlwain [1986] from ATS5 and ATS6  
2 observations at geosynchronous orbit, and (iii) the model of Weimer [1996] determined  
3 from ionospheric measurements; these empirical electric field models are respectively  
4 associated with (i) a centered dipole magnetic field, (ii) the M2 magnetic field determined  
5 from geosynchronous measurements, and (iii) Tsyganenko's [1996] magnetic field  
6 model determined from various statistical magnetometric in-situ measurements. These  
7 models will be briefly described in the next section.

8 In addition to a reliable magnetospheric electric field model, one needs also to have a  
9 correct physical theory for the formation of the plasmopause, i.e. a specific physical  
10 mechanism that accounts for the observations. Several such mechanisms have been  
11 proposed in the past and can be simulated numerically once an E-field model has been  
12 adopted.

13  
14 In the following sections we use the three E-field models mentioned above, and compare  
15 their influence on the dynamics of the plasmasphere during the geomagnetic storm on 28  
16 October 2001. Moreover, for the E5D model, the dynamical evolution of the cold plasma  
17 is tracked by using two different categories of simulations to predict the positions of the  
18 plasmopause and its deformations at different times precisely when EUV observations are  
19 available.

20  
21 There are other sophisticated models for the magnetospheric electric field distribution:  
22 for instance, AMIE developed by Richmond and Kamide [1988]. This popular E-field  
23 model was obtained from ground-based (magnetometer and radar) and ionospheric  
24 (DMSP satellite) data. Although it might be of some interest to use this additional model,  
25 it is not completely clear that ionospheric electric field distribution can be directly  
26 mapped up into the equatorial region of the magnetosphere where plasmopause knee start  
27 to form. Not only is the actual 3D distribution of magnetic field lines not completely  
28 guaranteed, but the existence of field-aligned electric potential drops is likely to  
29 jeopardize such a field-aligned mapping of ionospheric E-field into the magnetosphere.

30

1 In several studies, different convection electric field models have already been compared  
2 with observations [Jordanova et al., 2001; Boonsiriseth et al., 2001, Khazanov et al.,  
3 2004]. Their influence on the ring current was analyzed in detail by Chen et al. [2003].  
4 But their effects on particles of lower energies ( $<10$  eV) populating the plasmasphere was  
5 less well studied, except by Liemohn et al. [2004] who compared some electric field  
6 models, and their effects on plasmaspheric morphologies; he used (i) a modified  
7 McIlwain electric field model, (ii) the Weimer model, (iii) as well as another self-  
8 consistent electric potential model for the time span of the recovery phase of the 17 April  
9 2002 magnetic storm. These authors found that all these models have certain strengths  
10 but also some weaknesses in predicting the observed plasmopause position during this  
11 storm. They found especially that the electric field intensity of Weimer's model was a bit  
12 too strong in the inner magnetosphere, leading to a too small plasmasphere. Liemohn's  
13 modified McIlwain model (which differs from the original E5D model, and was not used  
14 with the associated M2 magnetic field model) has a too small electric field intensity  
15 around noon, leading to a plasmopause position that does not correspond to the EUV  
16 observations on the dayside although a good fit was obtained in the nightside.

17  
18 In the present work, we also present the results obtained during this magnetic storm of 17  
19 April 2002, but we have focused our attention on another clean and isolated geomagnetic  
20 storm: that observed on 28 October 2001. The VSMC, unmodified E5D and Weimer E-  
21 field models have been used with the hope to determine which of them might be the most  
22 appropriate for this magnetic storm.

23  
24 It is commonly assumed that the topologies of both the electric field and magnetic field  
25 determine the position where the plasmopause is formed at the time of geomagnetic  
26 storms and substorms. Postulating that the plasmopause coincides with the last closed  
27 equipotential of the magnetospheric electrostatic field distribution as proposed by Brice  
28 [1967], this led authors to derive an electric field topology from observed plasmopause  
29 positions: e.g. Maynard and Chen [1975]. This led also Goldstein et al. [2002] to add an  
30 electric field component penetrating into the plasmasphere to obtain plasmaspheric  
31 shapes and positions fitting those observed on 24 May 2000, when a plasmaspheric

1 shoulder was found in the EUV observations. In a subsequent study, Goldstein et al.  
2 [2003] included an additional E-field distribution related to sub-auroral polarization  
3 stream to obtain a better fit with plasmopause positions observed by EUV/IMAGE on 2  
4 June 2001.

5 The MHD simulations are essentially based on the postulate that the plasmopause  
6 coincides with the Last Closed Equipotential (LCE) of a stationary global  
7 magnetospheric electric field. When the magnetospheric electric field is not stationary,  
8 the plasmopause can not be identified with the LCE of the time-dependent E-field, but  
9 may be assumed to correspond to a Last Closed Streamline (LCS). This is what will be  
10 assumed in the MHD simulations presented below. The second mechanism used below to  
11 predict the plasmopause positions and shapes is based on the mechanism of interchange  
12 reported in the book by Lemaire and Gringauz [1998]. These mechanisms are recalled  
13 and described in section 3.

14  
15 In section 4, we illustrate the plasmopause positions simulated for all three different  
16 electric fields models and with both kinds of mechanisms. The results are then compared  
17 with observations of EUV/IMAGE. Discussion and conclusion are given in the last  
18 section.

## 19 20 **2. Models of electric and magnetic fields**

### 21 22 **2.1 Volland-Stern's and Maynard-Chen's convection electric field (VSMC)**

23  
24 The Volland-Stern model [Volland, 1973, Stern, 1975] is a simple mathematical model  
25 where a uniform dawn-dusk convection electric potential distribution is applied across  
26 the magnetosphere. It has become very popular because of its simplicity and portability.  
27 In this model there is no induced electric field resulting from time dependent magnetic  
28 field variations as can be envisaged during strong geomagnetic storms; the  
29 magnetospheric electric field derives from a scalar potential which, in a co-rotating frame  
30 of reference, is given by

$$31 \quad \Phi = AR^2 \sin \phi$$

1 where  $R$  is the equatorial radial distance,  $\phi$  is the azimuthal angle from noon and the Kp  
2 dependent factor  $A = \frac{0.045}{(1 - 0.159Kp + 0.0093Kp^2)^3} \left[ \frac{kV}{R_E^2} \right]$  determines the convection  
3 electric field intensity.

4  
5 The Kp dependence of this empirical model was obtained by Maynard and Chen [1975]  
6 by adjusting the last closed equipotential (LCE) of the total E-field with plasmapause  
7 positions determined by OGO3 and OGO5 satellite observations; this is why this model  
8 has been given the acronym VSMC in the following. The Kp dependence is very  
9 sensitive especially at small values of Kp; the value of  $A$  varies from  $A=45 \text{ V}/R_E^2$  for Kp  
10  $= 0$  to over  $800 \text{ V}/R_E^2$  for Kp = 6.

11  
12 Fig. 1 illustrates the equatorial contour maps of the equipotentials for the VSMC  
13 convection electric field every two hours from 0:00 UT to 10:00 UT during the  
14 geomagnetic storm of 28-10-2001. It shows how the dawn-dusk electric field component  
15 is shielded close to the Earth and how it is assumed to change over this 10h period.  
16 During this period of time, Kp increased from 1<sup>-</sup> at 0:00 UT to 7<sup>-</sup> at 05:00 UT, as  
17 illustrated in the top panels of Fig. 9.

18 In our simulations, this convection electric field is used with a centered dipolar magnetic  
19 field:  $B = \frac{3100}{R^2}$ . Indeed, this was the magnetic field assumed by Maynard and Chen

20 [1975] to compute the MHD convection velocity:  $\vec{E} \times \vec{B} / B^2$ .

21

## 22 **2. 2. McIlwain's E5D convection electric field**

23

24 Another analytical representation of the magnetospheric convection electric potential was  
25 derived by McIlwain [1986] from electron and proton dynamical spectra measured at  
26 geosynchronous orbit during the ATS-5 and ATS-6 missions:

27

$$\Phi = \left\{ R(0.8 \sin \phi + 0.2 \cos \phi) + 3 \right\} \left( 1 + 0.3 \frac{Kp}{1 + 0.1Kp} \right) \left( \frac{1}{1 + \left( 0.8 * \frac{R_{ar}}{R} \right)^8} \right)$$

$$\text{with } R_{ar} = 9.8 - 1.4 \cos \phi + (-0.9 - 0.3 \cos \phi) \frac{Kp}{1 + 0.1Kp}$$

The E5D model depends also on the three-hourly geomagnetic activity index Kp. It has been found in past statistical studies that this index controls the observed positions of the plasmopause, when the level of geomagnetic activity changes. Note however that, unlike the VSMC model, the E5D model was not derived by adjusting its parameters to fit observed plasmopause positions, but was directly deduced from ATS-5 and ATS-6 particle flux measurements at geosynchronous altitude, precisely in the region where the plasmopause is formed. The constants in the E5D electric potential model have been adjusted to fit the dynamical energy spectra in the range from 1 keV to 100 keV of electrons and protons injected following substorm events and observed in the equatorial region; according to McIlwain, this model is not necessarily reliable for Kp > 6, nor in the case of geomagnetic storms when rapidly changing electric field intensities are induced inside the magnetosphere.

It should be emphasized that McIlwain [1986] did not develop his E5D model based on ATS-5 and ATS-6 observations collected during geomagnetic storm events, when Dst has large excursions. In principle, this model is designed to simulate the plasmopause formation and deformations during relatively steady state conditions following substorm injection events. Nevertheless we will use it here during a geomagnetic storm with the caution that if the plasmopause positions predicted with this model would not fit adequately the observations during the geomagnetic storm, this may be due to the inadequacy of the E5D model to fit the actual electric field distribution during this period of time, and not necessarily to the inadequacy of the physical mechanism assumed to form the plasmopause.

1 Fig. 2 illustrates the equatorial equipotential contours for the E5D convection electric  
2 field model. These maps are shown every two hours of UT from 0:00 to 10:00 during the  
3 geomagnetic storm of 28-10-2001. It clearly indicates the shielding of the dawn-dusk  
4 electric field component near the Earth in the dawn sector. A comparison with Fig. 1  
5 indicates that the E5D electric field model is less sensitive to changes of Kp than the  
6 VSMC model.

7 To force a stronger Kp-variation, Liemohn et al [2001] re-scaled the E5D model to match  
8 the cross-polar cap potential difference to other types of observations. This led them to  
9 define a “modified McIlwain” E-field model that should no more support ATS-5 and  
10 ATS-6 observations. In our simulations, we keep the original E5D model, as well as the  
11 associated M2 equatorial magnetic field model since both were derived from concomitant  
12 ATS-5 and ATS-6 observations.

13 This M2 magnetic field model has a day-night asymmetry, and must be used in  
14 association with E5D to account for the actual day-night asymmetry of the convection  
15 velocities. Figure 3 illustrates the iso-contours of the equatorial magnetic field intensity  
16 corresponding to the M2 model. Beyond 5 earth radii, the deviations from a simple  
17 symmetric dipole become large especially in the nightside sector of the magnetosphere.  
18 Note that this B-field model does not depend on Dst nor on Kp unlike the model of  
19 Tsyganenko [1996]. Of course, this may be viewed as another limiting factor  
20 compromising its application to study the magnetic storm of October 28, 2001.

21

### 22 **2.3. Weimer’s convection electric field**

23

24 Unlike the two previous E-field models, Weimer’s model does not depend on the  
25 geomagnetic activity level Kp. Weimer's [1996] E-field model is driven by solar wind  
26 parameters: interplanetary magnetic field magnitude, solar wind velocity and dipole tilt  
27 angle. It was derived from low altitude ionospheric convection velocity measurements at  
28 high latitudes. Unfortunately, these observations are collected far from the equatorial  
29 region where the plasmapause is formed during substorm events.



1 Weimer electric potential [Weimer, 1996] is given by an expansion in spherical

2 harmonics: 
$$\Phi(\theta, \phi) = \sum_{l=0}^{\text{Min}(l,3)} (A_{lm} \cos m\phi + B_{lm} \sin m\phi) P_l^m(\cos\theta)$$

3 where  $\theta$  is a function of the geomagnetic co-latitude,  $\phi$  is the magnetic local time (MLT)  
4 and  $P_l^m$  are the associated Legendre functions. The coefficients  $A_{lm}$  and  $B_{lm}$  were derived  
5 by a least error fit from multiple satellite measurements of the ionospheric convection  
6 velocity.

7  
8 Fig. 4 illustrates the equatorial contour maps of Weimer's convection electric potential  
9 every UT hour from 00:00 UT up to 11:00 UT during the geomagnetic event of 28-10-  
10 2001. These equatorial isocontours of Weimer's equipotential are quite different from  
11 those illustrated in Figs. 1 and 2. The shielding is less efficient in the dawn sector than at  
12 dusk unlike in Fig. 2. From the distance between equipotential lines, it can also be seen  
13 that the electric field intensity is stronger than those illustrated in Figs. 1 and 2.

14 Moreover, Weimer's model depends on solar wind parameters varying over smaller time  
15 scales (60 minutes) and with larger amplitudes than the three-hourly index Kp controlling  
16 the VSMC and E5D models. Weimer's electric field intensity becomes especially strong  
17 in the dusk MLT sector at 4:00 UT at the beginning of the geomagnetic event while for  
18 the E5D model it is strongest in post-midnight sector (Fig. 2) and in both the dawn and  
19 dusk sectors for the VSMC model (Fig. 1).

20  
21 Weimer's electric field is used in association with Tsyganenko's [1996] magnetic field  
22 model that is controlled by the following input parameters: solar wind pressure, Dst, the  
23 Y and Z components of the interplanetary magnetic field, and the geodipole tilt angle.

#### 24 25 **2.4. Co-rotation electric field**

26  
27 To determine the total magnetospheric electric field in a non co-rotation frame of  
28 reference, the co-rotation electric field must be added to the convection electric field,  
29 postulating that these two E-field distributions could be superposed as in vacuum, despite  
30 the fact that the dielectric constant and permittivity of plasmas is much larger than that of

1 free space. However, according to Vasyliunas [2001] this assumption is questionable,  
2 since any (external) electric field imposed from outside of a plasma system does directly  
3 determine the convection velocity deep inside this plasma system. It is the plasma bulk  
4 motion and the generalized Ohm's law that determine the E-field inside the  
5 magnetosphere; this internal E-field distribution does not necessarily coincide with a  
6 'simple' superposition of the ionospheric co-rotation electric field, and an external  
7 convection electric field induced by the solar wind. Indeed, due to the large dielectric  
8 constant, the latter does not penetrate inside the magnetosphere. Although such a simple  
9 superposition in a plasma (i.e. a highly dielectric medium) is not consistent with classical  
10 electrodynamics of dielectric material, it seems, nevertheless, to approximate the actual  
11 magnetospheric E-field distribution with mitigated success, at least this is what was  
12 generally considered within the community.

13

14 The potential of the co-rotation electric field is given by:

15 
$$\Phi = -\frac{92}{R} [kV].$$

16

17 Note that it has been inferred from IMAGE observations that the azimuthal velocity of  
18 the plasmasphere is often slower (10% in average) than co-rotation in the outermost  
19 layers of the plasmasphere [Burch et al., 2004]. This effect has been tentatively taken into  
20 account in some simulations by reducing the co-rotation potential by this ad hoc factor  
21 [Pierrard, 2006]. In the present work, however, we will consider that co-rotation is  
22 applicable, since all three E-field models have been derived, originally, under such an  
23 assumption.

24 In any case, the co-rotation electric field dominates near Earth, where the equipotential  
25 lines are closed and almost circular. This is evidenced in Figs. 5, 6 and 7 showing the  
26 equatorial contour maps of the total electric potential in a non-corotating frame of  
27 reference, respectively for VSMC, E5D and Weimer's convection electric field models  
28 every two hours on 28 October 2001.

29

1 Note the significant differences between all three models. The last closed equipotential  
2 has a stagnation point at 18:00 MLT in the dusk sector for VSMC and E5D models, while  
3 it is located at later MLT, in the post-dusk local time sector, for Weimer's model. The  
4 LCE is everywhere closer to the Earth for the VSMC model than for the E5D one, for any  
5 value of the geomagnetic activity level  $K_p > 1$ .

6 The E-field intensity increases to larger value for the Weimer model than for the two  
7 other models during this geomagnetic storm. Therefore, the last closed equipotential  
8 penetrates closer to Earth for Weimer's model than for the two other models. For the  
9 VSMC model, the maximum E-field intensity is located in the morning sector (at 06:00  
10 MLT). In the E5D model, the maximum intensity is in the post-midnight sector (around  
11 2:00 MLT). Weimer's model also shows a maximum intensity in the post-midnight sector  
12 during the first hours preceding the geomagnetic storm similar to that displayed in the  
13 E5D model. During the storm main phase, this peak value moves closer to 06:00 MLT in  
14 both models.

15  
16 The evolution of the electric field (and magnetic field) in Weimer's model is controlled  
17 by the solar wind and geomagnetic parameters corresponding to 28 October 2001. Fig. 8  
18 shows the variation of the solar wind density of protons, the solar wind velocity and the  
19  $B_x$  and  $B_y$  components of the interplanetary magnetic field obtained from SPENVIS  
20 ([www.spennis.oma.be](http://www.spennis.oma.be)) from 27 to 30 October 2001. The three hourly  $K_p$ , hourly Dst  
21 and  $B_z$  values are given in the three top panels of Figs. 9 to 14.

22 Note that the 28 October 2001 storm is clearly associated to an increase of the solar wind  
23 velocity and density. Moreover, like most geomagnetic storms it is initiated by a  
24 southward turning of the interplanetary magnetic field direction. The geomagnetic  
25 activity level  $K_p$  index increases up to 7. The Dst index decreases by more than 150 nT.

### 27 **3. Dynamical simulations**

#### 29 **3. 1. Ideal MHD simulations**

1 Different mechanisms have been proposed to form plasmaspheric “knee” or plasmopause.  
2 These mechanisms are described in detail in the book by Lemaire and Gringauz [1998].  
3 The early theoretical MHD simulations by Grebowsky [1970] predicted that the evolution  
4 of the plasmopause is determined by the ideal MHD motion of the LCE at an arbitrarily  
5 chosen initial time  $t_0$ . In Grebowsky’s early dynamical simulations, the plasmopause was  
6 assumed to coincide with the LCE surface at  $t_0$ . But at any subsequent instant of time, the  
7 plasmopause did not coincide with the LCE of the changing convection E-field, unless  
8 the magnetospheric convection electric field would be independent of time.  
9 Our ideal MHD simulations differ from those of Grebowsky. They resemble more closely to  
10 those developed by Rasmussen [1992]. We launch plasma elements at 23:00 MLT, every  
11 0.15 Re at radial distances ranging from 1.2 to 6 Re along an equatorial radius. The drift  
12 path of these ideal MHD plasma elements are calculated from  $\vec{E} \times \vec{B} / B^2$  where  $\vec{E}$  and  $\vec{B}$  are  
13 respectively the electric field and the magnetic field given by the adopted models. We let the  
14 plasma drift around the Earth for 24 h, and determine the last closed streamline (LCS) which  
15 is then used as the initial plasmopause position at time  $t_0$ . The ideal MHD drift path of all  
16 plasma elements proceeds until a time when EUV observations are available and can be used  
17 for comparison. Plasma elements are continuously launched from 23:00 MLT every 5  
18 minutes, and tracked until they are deviated near the stagnation point, and are eventually lost  
19 at the magnetopause; we stop tracking any plasma element once it has completed one turn  
20 around the Earth. The equation of motion of each plasma element is integrated by a Runge-  
21 Kutta method with an adapted time step to satisfy a correct numerical accuracy; the  
22 equatorial positions of all plasma elements are stored every 5 min to map the deformations of  
23 the LCS as a result of Kp variations. For these ideal MHD simulations the LCS is assumed to  
24 coincide with the plasmopause; it should be reminded that the LCS does not coincide at any  
25 time with the LCE of the convection electric field.  
26  
27 In the regions close to the Earth where co-rotation is enforced, the plasmaspheric plasma is  
28 always highly coupled with that of the ionosphere. Since all flux tubes are on closed  
29 streamlines in this region, they are assumed to be completely full, and their densities are  
30 given by the empirical model of Carpenter and Anderson [1992]:

1  $\log_{10} N_{eq} = -0.3145L + 3.9043$  where  $N_{eq}$  is the number density in electrons/cm<sup>3</sup> in the  
2 equatorial plane; it is independent of the local time angle, but it is a function of the McIlwain  
3 parameter L. Note also that it does not depend on the level of geomagnetic activity.

4 The plasma elements located further away from the Earth are more significantly affected by  
5 the solar wind induced magnetospheric convection. When the convection electric field is  
6 enhanced during periods of substorm injection events, the core of the plasmasphere where  
7 co-rotation dominates shrinks. The outer flux tubes beyond the last closed streamline (LCS)  
8 are eventually depleted in less than 24 hours. When the convection electric field intensity  
9 decreases, the outer flux tubes can gradually refill with cold plasma flowing up from the  
10 ionosphere.

11  
12 Figs. 9 (three upper panels) illustrate the results of these MHD simulations for 28 October  
13 2001 at 00:00 UT for the three electric field models described above. In the all following  
14 Figures, the upper left panels show the results for the E5D model; upper middle panels those  
15 for VSMC model, and upper right panels for Weimer's model. The symbols represent the  
16 plasma elements corresponding to the flux tube contents that were launched at 23:00 MLT 24  
17 hours before  $t_0$ . At small radial distances, the symbols form concentric circles corresponding  
18 to a contour of constant density content. At large radial distances, the contours of constant  
19 tube content become elongated in the pre-dusk sector, indicating a decrease of the number  
20 density in this sector. Bottom left panel in Fig. 9 corresponds to the result of the simulation  
21 based on the interchange mechanism for the formation of the plasmopause and E5D E-field  
22 model.

23  
24 We compare the successive positions of the plasmopause found with the MHD  
25 simulations assuming each point moves with the instantaneous  $\vec{E} \times \vec{B} / B^2$  drift velocity  
26 calculated with the three different E-field models: VSMC, E5D, and Weimer. Note that  
27 this convection velocity is never parallel to the equipotential lines of these models unless  
28 the E-field and B-field would both be stationary. Due to the continuously changing E-  
29 field distribution, the position of the LCS is a function of time. Let us recall that the LCS  
30 corresponds to the envelope of all drift paths that have not reached the magnetopause

1 boundary during the previous 24 hours. This is why it should be denoted LCS-24h. A  
2 different LCS could have been obtained if the closure time would have been 25 hours, 2  
3 days, 3 or 6 days as in the MHD simulations of Chen and Wolf [1972].  
4 The position of the LCS-24h found with our MHD simulations corresponds to the boundary  
5 where the number of plasma elements per unit area decreases sharply in Figs 9 to 15 (except  
6 at 23:00 MLT and beyond where new plasma elements are continuously launched every five  
7 minutes). If the plasmopause is identified with one of the last closed streamlines, it should be  
8 specified what is the closure time that has been adopted in the MHD simulations. This means  
9 that the location of the plasmopause, a physical boundary, would depend on the arbitrary  
10 choice of a closure time in any MHD simulation. This is clearly a conceptual limitation of the  
11 plasmopause with the LCS and even worse with the LCE.

12  
13 Figs. 9 to 14 show that a plume is produced in the dusk sector during the magnetic storm in  
14 all three MHD simulations. This plume in the LCS-24h is similar to that observed by  
15 EUV/IMAGE after 18:00 UT.

16 Fig. 10 shows that at 04:30 UT, the LCS-24h has been pushed inwards in the nightside  
17 region. Although the EUV observations show also an inward shift of the plasmopause near  
18 midnight, the overall shape of the plasmasphere is however very different from that of the  
19 LCS-24h obtained with the MHD simulations. While the LCS has rather smooth and regular  
20 shape, the actual plasmopause is much more indented and irregular. This can be a  
21 consequence of the rather poor time resolution of the Kp index controlling the E-field  
22 distributions. Since the magnetospheric E-field is changing over smaller time scale, the actual  
23 MLT variation of the LCS is expected to be more irregular than illustrated in Figs. 10 to 14.  
24 Another important consequence of the shorter time variation of the E-field distribution, and  
25 of the associated plasma flow which must be quite variable, was pointed out by Dungey  
26 [1967] soon after the discovery of the sharpness of "Carpenter's knee". He wrote : " Some  
27 tubes of high density (i.e. from inside the plasmasphere) should sometimes be swept out on  
28 the day side, and some tubes, after entering from the tail, should enter the inner region and,  
29 after a few days, should have intermediate values of density. It then seems rather surprising  
30 that the knee should be so sharp, but the variable model would predict a patchy density in the  
31 region near the knee and this could be the true state" (sic). We share Dungey's early concern

1 about the sharpness of a knee along the LCS. The short time scale variability of the  
2 magnetospheric plasma flow does not support the formation of sharp density gradients like  
3 those observed soon after the peeling off of the plasmasphere which are associated with  
4 substorm events or inward motion of injection boundaries. However, the variability of the  
5 magnetospheric plasma flow may well account for the existence of the Plasmasphere  
6 Boundary Layer where Carpenter and Lemaire [2004] identified patchy plasma density  
7 irregularities.

8  
9 Note that the LCS corresponds in the MHD simulations of Chen and Wolf [1972] to the  
10 limit between magnetic flux tubes which have refilled for more than 24 hours and those  
11 that have refilled for less than 24 hours. If such a limit should correspond to the actual  
12 plasmopause, it must be admitted that the position of this physical boundary would  
13 depend on the choice of the refilling time which in our simulations was arbitrarily taken  
14 to be 24 hours. In Chen and Wolf's MHD simulations different plasmopause locations  
15 were obtained when the refilling time was assumed to be 6 days, 5 days, 4 days, 3 days, 2  
16 days or 24 hours.

17 This illustrates again the drastic limitation of identifying the plasmopause by any kind of  
18 MHD simulations whose results depend on an arbitrary choice of the closure time and a  
19 refilling time. Furthermore, the results of these MHD simulations rely also on the  
20 arbitrary choice of the initial time,  $t_0$ , when such simulations are assumed to start, and on  
21 the assumption of the density distributions in all flux tubes at this starting time.

22

### 23 3.2. Interchange mechanism

24 Another mechanism has also been proposed for the formation of the plasmopause: the  
25 interchange mechanism, illustrated by Lemaire and Kowalkowski [1981]. According to  
26 this mechanism, the plasma becomes unstable above a Zero Parallel Force (ZPF) surface  
27 where the parallel component of the gravitational plus centrifugal accelerations is equal  
28 to zero [Lemaire, 1985, 2001]. This occurs in the nightside local time sector during  
29 substorms and storms at an equatorial distance that depends on the distribution of the  
30 convection velocity. The plasmasphere is peeled off in this sector by the centrifugal effect  
31 which is enhanced when the convection velocity is enhanced beyond the inner edge of a

1 substorm injection boundary. By this mechanism, a new plasmopause forms closer to the  
2 Earth than the LCS determined by the MHD simulations presented and discussed above.  
3 This mechanism has been used in numerical simulations performed by Lemaire [1985,  
4 2000] and by Pierrard and Lemaire [2004]. The positions of the plasmopause predicted by  
5 this mechanism with the E5D model have been compared to observations of IMAGE for  
6 typical dates [Pierrard and Cabrera, 2005, 2006; Pierrard, 2006].

7  
8 In these non-MHD simulations based on the interchange mechanism, plasma holes with a  
9 density smaller than the background density are launched at 23:00 MLT in the equatorial  
10 plane. Due to the interchange motion, these holes drift ultimately toward an asymptotic  
11 trajectory where the radial component of the gravitational force and centrifugal force  
12 balance each other. This corresponds to the Zero Radial Force (ZRF) surface. However,  
13 the parallel components of these forces balance each other closer to the Earth along a  
14 virtual surface that Lemaire [1985] has called the Zero Parallel Force (ZPF) surface. It is  
15 assumed that the field aligned plasma distribution becomes convectively unstable along  
16 all flux tubes that traverse or are tangent to this virtual ZPF surface. In these flux tubes  
17 field aligned flow velocity is enhanced, and the plasma density is reduced due to its  
18 upward expansion. For a dipole magnetic field distribution the equatorial distance of the  
19 ZPF is  $3^{2/3}$  time smaller than that of the ZRF surface. We assume that for the M2  
20 magnetic field model the minimum equatorial distance of the ZPF surface is also  
21 approximately  $3^{2/3}$  times smaller than that of the ZRF surface, as it is for a dipole B-field.

22  
23 At time  $t_0$  we start with a plasmopause whose position has been determined at all MLT  
24 angles by the history of the geomagnetic activity level during the previous 24 h. Note that  
25 the simulations could also be started by using an observed plasmopause position at the  
26 time  $t_0$  like in the study of Goldstein et al. [2003]. This procedure would of course favor  
27 the agreement between the results of the simulation and the observations at any  
28 subsequent times. Unfortunately, this procedure does not tell us about the physical  
29 mechanism that has formed this initial plasmopause; it may only be useful to test the  
30 appropriateness of the E-field models chosen in simulations, after the plasmopause had  
31 already formed.



1  
2  
3  
4  
5  
6  
7  
8  
9  
10  
11  
12  
13  
14  
15  
16  
17  
18  
19  
20  
21  
22  
23  
24  
25  
26  
27  
28  
29  
30  
31

In the next section, we describe and compare the results obtained with the following series of simulations: MHD with the E5D model (MHD E5D), MHD with the Volland-Stern-Maynard-Chen model (MHD VSMC), MHD with the Weimer model (MHD W), and interchange with E5D model (IC E5D).

**4. Discussion of the results**

**4.1 Magnetic storm of 28-10-2001**

Figs. 9 to 14 illustrate the equatorial position of the plasmopause obtained with two different mechanisms for the formation of the plasmopause and three different electric field models, respectively at 0:00, 4:30, 8:00, 12:00, 18:00 and 20:00 UT. The simulations correspond to MHD E5D (left upper panels), MHD VSMC (middle upper panels) and MHD W (right upper panels). The results obtained with the interchange mechanism and the E5D model are also presented in the left bottom panel d of these graphs. The plasmopause found with the interchange mechanism is closer to Earth than with MHD simulations when a same E-field model is used. We do not provide simulations with interchange mechanism for the other electric field models since this would prohibitively increase the size of this paper without improving significantly its main results. Note also that the use of the interchange mechanism would not be physically significant in association with an E-field like the VSMC model which has been fitted in order to match the LCE with observed plasmopause positions.

The top panels of Fig. 9 to 14 illustrate the Kp and Dst indices and the northward component of the interplanetary magnetic field (Bz) from the beginning of 27-10-2001 to the end of 29-10-2001. At 00:00 UT, the level of geomagnetic activity is very low (Kp = 1) and increases to 7 over the next 3 hours when the main phase of the geomagnetic storm starts, i.e., when Dst begins a gradual drop, as shown on Fig. 9.

At 04:39, 08:03, 18:05 and 19:58 UT, there are exploitable observations from the EUV instrument since the orbit of the satellite IMAGE is close to its apogee. These images are.

1 presented in the bottom right panels of Figs. 10, 11, 13 and 14, respectively. These  
2 observations are intensity maps of the 30,4 nm emissions of Helium ions integrated along  
3 the line of sight. They are projected in the geomagnetic equatorial plane in the SM  
4 coordinate system with the program XForm available at  
5 (<ftp://euv.lpl.arizona.edu/pub/bavaro/unsupported/>). This software tool enables to view  
6 the plasmopause cross section from over the North Pole like in our simulations. The  
7 plasmopause is assumed to be the sharp edge where the brightness of 30.4 nm He<sup>+</sup>  
8 emissions drops drastically. This boundary is illustrated by a white line corresponding to  
9 a threshold equal to 40% of the maximum light intensity.

10  
11 Just before the storm, the MHD E5D simulation predicts at 00:00 UT a plasmasphere  
12 extending up to 6 Re. Since the dawn-dusk component of the two other convection  
13 electric fields (VMSC and Weimer) are stronger than that of the E5D model, the LCS is  
14 located closer to the Earth for these two other models: i.e. around 4 Re for the MHD  
15 VSMC, and even closer for the MHD W simulation. When the interchange mechanism is  
16 assumed to peel off the plasmasphere, the plasmopause at midnight LT is located around  
17 4.5 Re with the E5D model; this is closer to Earth than the LCS simulation for this same  
18 E-field model. However, the plasmopause predicted by the IC E5D simulation is located  
19 at larger equatorial distances than the LCS for the two other E-field models. But for a  
20 same E-field model, the minimum equatorial distance of the ZPF surface is generally  
21 smaller than that of the LCS.

22  
23 Note that the plasmasphere is almost circular at that time which corresponds to the initial  
24 time  $t_0$  in all different simulations. Although the level of geomagnetic activity has been  
25 nearly constant and quite low during the previous 24 h, a bulge is present at  $t_0$  in the dusk  
26 sector in the MHD VSMC simulation. However, according to the EUV observations the  
27 plasmasphere is usually circular after prolonged quiet periods. Plasma tails or plumes are  
28 formed only during disturbed periods [Pierrard and Cabrera, 2005]. Unfortunately, no  
29 observations of EUV/IMAGE are available at 00:00 UT 28 October 2001, since the  
30 satellite was not close to its apogee at that initial time  $t_0$ .

31

1 At 04:30 UT as illustrated in Fig. 10, the geomagnetic activity level  $K_p$  increases  
2 significantly and reaches a maximum  $K_p = 7$ . This increase of  $K_p$  is associated to a  
3 southward turning of the interplanetary magnetic field  $B_z$ , as well as a decrease of Dst  
4 index. The latter reaches a minimum of  $-157$  nT at 11:00 UT. By that time, the  
5 convection electric field intensity has increased in all models so that the corresponding  
6 LCS-24h are less extended. Only the innermost flux tubes have a circular trajectory,  
7 while the more distant closed streamlines are highly skewed with a maximum radial  
8 distance in the post-noon sector. Beyond the LCS, the plasma elements are lost to the  
9 magnetosheath and are not any longer tracked in our MHD simulations. According to this  
10 MHD theory for the formation of the plasmopause, a more or less sharp knee is formed  
11 along the LCS-24h, wherein the streamlines have remained closed for at least 24 hours.  
12 The LCS shrinks to about  $3 R_e$  in the night sector for all MHD simulations. A bulge is  
13 formed in the afternoon sector for all the simulations as a result of the enhancement of the  
14 dawn-dusk E-field component. Indeed, this enhancement of E-field in the dusk sector  
15 produces a sunward surge of plasma in this MLT sector. Note, however, the quite  
16 different shapes of the equatorial cross section of the LCS predicted by the various E-  
17 field models. The bulge in the LCS is the precursor of the plume that usually develops  
18 during geomagnetic storms and substorms.

19  
20 The interchange mechanism shown in the fourth panels produces much more irregular  
21 plasmopause shapes than the MHD simulations. From the fourth panel in Fig. 10, it can  
22 be seen that the ZPF surface where the plasmasphere is peeled off in the postmidnight  
23 sector corresponds to an equatorial distance slightly beyond  $2 R_e$ . Despite the rather  
24 limited quality of the observations of IMAGE at the time of 04:30 UT, it can be seen that  
25 the plasmopause is located close to the Earth during this storm.

26  
27 At 08:00 UT, the  $K_p$  index is still high:  $K_p = 6$ . As illustrated in Fig. 11, a plume is now  
28 clearly developed in all the simulations, with and without interchange. The plumes are  
29 located in the afternoon sector but have rather different shapes and experience quite  
30 different development depending on the adopted E-field model. The observation of

1 EUV/IMAGE at 08:03 UT is very contaminated, but a plume can clearly be identified in  
2 the afternoon sector.

3 With MHD VSMC and Weimer simulations, the plasmasphere is still smaller than with  
4 MHD E5D, due to their stronger dawn-dusk E-field intensity which implies a stagnation  
5 point rather close to Earth. The simulation of interchange with the E5D model, gives a  
6 position of the plasmopause which is rather close to that of the LCS of MHD E5D  
7 simulation.

8  
9 By 12:00 UT, the plume observed in the simulations has slightly rotated eastward as can  
10 be seen in Fig. 12. No EUV observations are unfortunately available at that time. At  
11 18:05 and 19:58 UT, EUV/IMAGE provides nice observations, and a plume is clearly  
12 visible in the afternoon/dusk region as illustrated in Figs. 13 and 14. The results of the  
13 simulations are also shown for 18:00 and 20:00 UT. The longitudinal extent and MLT  
14 position of the plume is again slightly different in the different models. Note that by  
15 reducing arbitrarily the co-rotation velocity, a better agreement would be obtained. This  
16 kind of forcing has been avoided in the present work in order not to distort the original E-  
17 field models which have been derived without reducing the co-rotation electric field  
18 intensity. Note nevertheless that the velocity of the plasmasphere is observed to be  
19 generally slower than co-rotation [Burch et al., 2004], what explains the faster rotation of  
20 the plume in the different simulations compared to the EUV observations.

21  
22 Similar plumes are often observed by EUV/IMAGE and CLUSTER after a significant  
23 increase of the geomagnetic activity level [Darrouzet et al., 2006a and b]. They are  
24 formed in the afternoon sector and then rotate eastward with the core of the  
25 plasmasphere. Other examples of IMAGE observations during quiet and disturbed  
26 periods that have been compared to results of simulations based on the interchange  
27 mechanism (IC E5D) have been presented by Pierrard and Cabrera [2005, 2006] and  
28 Pierrard [2006].

## 30 **4.2 Magnetic storm of 17 April 2002**

1 Fig. 15 shows the results of similar simulations obtained during the geomagnetic storm of  
2 17-4-2002. This case is particularly interesting since this is the single event for which the  
3 effect of several electric field models on the position of the plasmopause has been also  
4 determined by Liemohn et al. [2004]. The E-field models tested in this paper were (i)  
5 their modified E5D model rescaled to have a larger intensity than McIlwain's original  
6 version, (ii) the Weimer model, and (iii) a self consistent E-field determined by the  
7 authors. Thus it is interesting to compare the results of the present MHD simulations  
8 based on VSMC as well as on the original E5D model version with the results found by  
9 Liemohn et al. [2004] for the same event on 17-4-2002 with other E-fields models.  
10 Moreover, we also show the effect of the interchange mechanism on the positions, shape  
11 and evolution of the plasmopause during this magnetic storm.

12  
13 Fig. 15 shows the results at 21:00 UT on 17-4-2002 obtained with the MHD simulations  
14 respectively for E5D, VSMC and Weimer models (three upper panels), as well as with  
15 interchange mechanism based on the E5D model (left bottom panel). A plume is again  
16 formed with all the electric field models. Its development is associated to the increase of  
17 the geomagnetic activity level up to  $K_p = 7^+$ . This increase of  $K_p$  is also associated with a  
18 southward turning of the interplanetary magnetic field, like during all geomagnetic  
19 storms. During the main phase, Dst decreases reaching a minimum of -105 nT on 17-4-  
20 2002 and even a lower value the day after. The plume is located approximately in the  
21 same MLT sector as in the observations of EUV. The MHD E5D simulation shows a  
22 plasmopause quite similar to that obtained with the rescaled E5D model used by Liemohn  
23 et al. The position of the plasmopause found in Liemohn et al. MHD simulation was in  
24 good agreement with the observations of EUV in the nightside, but it was too far from the  
25 Earth on the dayside. We obtain the same characteristics with the MHD E5D simulation.  
26 The MHD VSMC simulation corresponds better to the plasmopause observations on the  
27 dayside, but on the nightside, it is too close from the Earth. The MHD W simulation  
28 based on Weimer model gives also a plasmopause closer to the Earth than what is  
29 observed, especially on the nightside; these results are in agreement with the simulation  
30 published by Liemohn et al. where the Weimer convection E-field is also used.

31

1 The simulation of the interchange mechanism with the E5D model gives results closer to  
2 the EUV observations than the MHD simulations with this same E5D electric field  
3 model. This does not imply, of course, that there is no need for better E-field model than  
4 E5D, nor is it a pleading for the mechanism of interchange, since any physical theory is  
5 necessarily an approximation and is therefore perfectible.

6  
7 While in general, interchange simulations with E5D model predict results that are in good  
8 agreement with the EUV observations during substorm events [Pierrard and Cabrera,  
9 2005], we have seen here that such an agreement is more precarious during the  
10 geomagnetic storms examined in this paper. We attribute the lack of satisfactory results  
11 during geomagnetic storms to the lack of characterization of the E5D electric field model  
12 under this sort of geomagnetic disturbances. Indeed, this empirical E-field model was not  
13 designed to reproduce the magnetospheric convection electric field during geomagnetic  
14 storms, but only to model the dispersion of electrons and protons accelerated or injected  
15 into the magnetosphere following substorm events [McIlwain, 1986]. This lays the need  
16 to update and improve currently available empirical electric field models not only at  
17 ionospheric level but also at high altitudes in the Earth magnetosphere. Furthermore,  
18 nobody can argue that future alternative theories for the formation of the plasmopause  
19 will not be able to simulate the dynamics of the plasmasphere more accurately and offer  
20 predictions in closer agreement with observational reality.

## 21 22 **5. Conclusions**

23  
24 After brief descriptions of different electric fields models (: the Volland-Stern-Maynard-  
25 Chen model VSMC, McIlwain's E5D model and the Weimer model), we first determined  
26 how the distribution of the equatorial equipotentials corresponding to these  
27 magnetospheric convection E-field models change during the geomagnetic storm of 28  
28 October 2001. Their equipotentials in co-rotating and non-corotating frames of reference  
29 depend on the level geomagnetic activity; they are thus changing as a function of  
30 universal time since the geomagnetic activity indexes Kp and Dst are varying hour after  
31 hour.

1 The radial and local time distributions of these equipotential contours have been  
2 displayed in Figs. 1, 2, 4, 5, 6, and 7 for a set of times for which EUV observations are  
3 sometimes available. The E-field models are used in association with magnetic field  
4 models (VSMC/dipole, E5D/M2 model, and Weimer/Tsyganenko respectively), to  
5 calculate the convection velocity of cold plasma or the drift velocity of zero energy  
6 charged particles. The dipolar and M2 magnetic field models had been employed to  
7 design, respectively, the VSMC and E5D models from in-situ satellite observations. In  
8 addition to their portability, these simple quasi-stationary E-field models have an  
9 expedient advantage: they depend only on one single parameter, the three-hourly Kp  
10 geomagnetic activity index. This makes them user friendly and easy to implement in any  
11 numerical codes. Weimer E-field is more sophisticated: it depends on several solar wind  
12 parameters and varies with a smaller time resolution. Nevertheless, it is based on low  
13 altitudes and high latitudes observations collected far from the equatorial region where  
14 the plasmopause is formed.

15 Although all these empirical electric field models are based on observations (respectively,  
16 on OGO-3 & 5 satellites for VSMC, AST-5 & 6 satellites for E5D and low altitude  
17 ionospheric convection velocity measurements at high latitudes for Weimer), they occur  
18 to be quite different from each other. Note that these models are averages and  
19 approximations of the actual field distributions at any particular instant of time, and at  
20 any particular place in the magnetosphere. Some of them were not designed to model  
21 magnetospheric electric fields in cases of rapidly changing magnetic field intensities: e.g.  
22 during geomagnetic storms when induction electric fields are generated on top of the  
23 electrostatic component approximated by these E-field models. For instance, the E5D  
24 model was essentially built to represent the E-field distribution immediately after a  
25 substorm injection event; furthermore, it was developed to represent the E-field in the  
26 region of geosynchronous orbit, only when the level of geomagnetic activity, denoted by  
27 the value of Kp, remains nearly constant and smaller than 6. McIlwain's electric field  
28 E5D was not developed under such circumstances as geomagnetic storms. But, taking  
29 into account these warnings and restrictions, it is interesting to note that the plasmopause  
30 position obtained with this E-field model and the IC mechanism is in better agreement

1 with the EUV observations during the geomagnetic storm of 17 April 2002 than the  
2 positions obtained with the other E-fields models and MHD simulations.

3  
4 Two mechanisms of plasmopause formation were also compared and confirm that the  
5 last-closed-streamline (LCS) of the MHD simulation is located beyond the plasmopause  
6 predicted by the interchange mechanism for the geomagnetic storm of October 28, 2001:  
7 the latter being thus generally closer to the Earth. A similar comparison with results  
8 obtained for the geomagnetic storm of April 17, 2002 leads to the same conclusions.

9  
10 The choice of the E-field model is crucial in the results of the simulations. Plumes  
11 develop during geomagnetic storms and substorms with all the various E-field models,  
12 but quite different shapes of the equatorial cross section of the LCS are predicted. It is  
13 quite clear that more detailed magnetospheric E-field models with higher time resolutions  
14 should be developed. In such future E-field models the distribution of the equipotential  
15 surfaces should possibly be desynchronized: their evolution in the night side should not  
16 necessarily be synchronized with that in the dayside or at any other MLTs. Finally, it  
17 would be useful to model also the inductive electric field component in order to model  
18 more properly what happens during geomagnetic storms.

19 Despite the better scores of the E5D electric field model and of the interchange scenario  
20 for the formation of the plasmopause found in many case studies, it must be admitted,  
21 however, that the equatorial cross section of the plasmopause as determined from the  
22 EUV observations during both geomagnetic storms, are not very well reproduced by none  
23 of the simulations presented above, not even when the Weimer electric field model is  
24 used instead of the E5D model. This leads us to conclude that none of the electrostatic  
25 field models is fully adapted to model the actual magnetospheric E-field distribution  
26 during geomagnetic storms (at least for those selected in the present study).

27  
28 Since previous simulations by Pierrard and Lemaire [2004] as well as by Pierrard and  
29 Cabrera [2005] based on the interchange mechanism and the E5D electric field model  
30 have shown that overall shapes of the plasmopause and its evolution does rather well  
31 explain the formation of plasmatails or plumes as well as shoulders following to



1 substorm events, it may be speculated that during geomagnetic storms characterized by  
2 larger Dst variations, the time dependent electric field distribution has an induced  
3 component associated to the increase of southward magnetic field which is generated by  
4 the Ring Current during the main phase. A toroidal induced electric field of smaller  
5 intensity and of opposite direction is also expected during the recovery phase of  
6 geomagnetic storms. These toroidal induced electric fields cannot be represented as the  
7 gradient of a scalar electrostatic potential as most empirical magnetospheric E-field  
8 models used above. The effect of such additional time dependent and non curlfree electric  
9 field distribution on the plasmasphere and on the formation of the plasmopause, has not  
10 yet been evaluated in detail.

11 It is suggested here that such induced electric fields generated during geomagnetic storms  
12 are responsible for the lack of satisfactory agreement between the simulations presented  
13 in this study based on curlfree electric field models. We suggest that this effect should be  
14 examined in the future and included in forthcoming and more comprehensive theories  
15 for the formation of the plasmopause not only during substorm events but also even  
16 during geomagnetic storms with large Dst variations.

17  
18 Therefore, this study points out the need to develop higher time resolution empirical  
19 models for the magnetospheric electrostatic field distribution like those developed for the  
20 geomagnetic field. It urges to take into account the effect of induced electric fields  
21 generated in the magnetosphere during geomagnetic storms with large Dst variations. It is  
22 only when such more detailed and comprehensive E-field models will be available in  
23 association with the time dependent empirical B-field models, that one might expect to  
24 test quantitatively and more definitely any of the existing and future theories for the  
25 formation of the plasmopause by comparing their theoretical predictions to observations  
26 like those of EUV.

## 27 28 Acknowledgements.

29 The authors thank the Belgian Science Policy office (SPP) for supporting this study.  
30

## 31 32 References

- 1  
2 Albert, J. M. (2003), Evaluation of Quasi-Linear Diffusion Coefficients for EMIC Waves in a Multispecies  
3 Plasma, *J. Geophys. Res.*, 108, NO. A6, 10.1029/2002JA009792.  
4
- 5 Baker D.N., S.G. Kanekal, X. Li, S.P. Monk, J. Goldstein, and J.L. Burch (2004), An extreme distortion of  
6 the Van Allen belt arising from the "Halloween" storm in 2003. *Nature* 432, 878, doi:10.1038/nature03116.  
7
- 8 Boonsiriseth A., R. M. Thorne, G. Lu, V. K. Jordanova, M. F. Thomsen, D. M. Thomsen, D. M. Ober, and  
9 A. J. Ridley (2001), A semiempirical equatorial mapping of AMIE convection electric potentials (MACEP)  
10 for the January 10, 1997, magnetic storm, *J. Geophys. Res.*, 106, 12903-12917.  
11
- 12 Brice, N. M. (1967), Bulk motion of the magnetosphere, *J. Geophys. Res.*, 72, 5193-5211.  
13
- 14 Burch J. L., J. Goldstein, and B. R. Sandel (2004), Cause of plasmasphere corotation lag, *Geophys. Res.*  
15 *Lett.*, 31, L05802, doi: 10.1029/2003GL019164.  
16
- 17 Carpenter, D. L., and R. R. Anderson (1992), An ISEE/whistler model of equatorial electron density in the  
18 magnetosphere, *J. Geophys. Res.*, 97, A2, 1097-1108.  
19
- 20 Carpenter, D. L., and J. Lemaire (2004), The plasmasphere boundary layer, *Annales Geophys.*, 22: 4291-  
21 4298.  
22
- 23 Chen M. W., M. Schulz, G. Lu, and L.R. Lyons (2003), Quasi-steady drift paths in a model magnetosphere  
24 with AMIE electric field: Implications for ring current formation, *Journal of Geophysical Research* Vol.108  
25 N.A5, 1-19.  
26
- 27 Chen A. J., and R. A. Wolf (1972), Effects on the plasmasphere of time-varying convection electric field,  
28 *Planet. Space Sci.*, 20, 483-509.  
29
- 30 Cornwall J. M., H. H. Hilton, and P. F. Mizera (1971), Observations of Precipitating Protons in the Energy  
31 Range  $2.5 \text{ keV} < E < 200 \text{ keV}$ , *J. Geophys. Res.*, Vol. 76, p. 5220.  
32
- 33 Darrouzet F., J. De Keyser, P. M. E. Décréau, D. L. Gallagher, V. Pierrard, J. F. Lemaire, B. L. Sandel, I.  
34 Dandouras, H. Matsui, M. Dunlop, J. Cabrera, A. Masson, P. Canu, L. Rauch, and M. André (2006a),  
35 Plasmaspheric plumes: CLUSTER, IMAGE and simulations, *Proceedings of the Cluster and Double Star*  
36 *Symposium, 5th anniversary of Cluster in Space, 1-6, (ESA ESTEC, Noordwijk, The Netherlands, 19-23*  
37 *September 2005) ESA SP-598.*  
38
- 39 Darrouzet F., J. De Keyser, P. M. E. Décréau, D. L. Gallagher, V. Pierrard, J. F. Lemaire, B. R. Sandel, I.  
40 Dandouras, H. Matsui, M. Dunlop, J. Cabrera, A. Masson, P. Canu, J. G. Trottignon, J. L. Rauch, and M.  
41 André (2006b), Analysis of plasmaspheric plumes: CLUSTER and IMAGE observations, *Annales*  
42 *Geophys.*, 24, 1737-1758.  
43
- 44 Dungey, J.W. (1967), The theory of the quiet magnetosphere, in *Proceedings of the 1966 Symposium on*  
45 *Solar-Terrestrial Physics*, Belgrade, eds King, J.W. and Newman, W.S., pp. 91-106.  
46
- 47 Goldstein J., B. R. Sandel, M. R. Hairston, and P. H. Reiff (2003), Control of plasmaspheric dynamics by  
48 both convection and subauroral polarization stream, *Geophys. Res. Lett.*, 30, 24, 2243,  
49 doi:10.1029/2003GL018390.  
50
- 51 Goldstein J., R. W. Spiro, P. H. Reiff, R. A. Wolf, B. R. Sandel, J. W. Freeman, and R. L. Lambour (2002),  
52 IMF-driven overshielding electric field and the origin of the plasmaspheric shoulder of May 24, 2000,  
53 *Geophys. Res. Lett.*, 29, 16, 10.1029, 66-1:4.  
54
- 55 Grebowsky, J. M. (1970), Model study of plasmopause motion, *J. Geophys. Res.*, 75, 4329-33.  
56

- 1 Jordanova V. K., L. M. Kistler, C. J. Farrugia, and R. B. Torbert (2001), Effects of inner magnetospheric  
2 convection on ring current dynamics, March 10-12, 1998, *J. Geophys. Res.*, 106, 29705.  
3
- 4 Khazanov, G. V., K. Gamayunov, D. L. Gallagher, and J. U. Kozyra (2006), Self-consistent model of  
5 magnetospheric ring current and propagating electromagnetic ion cyclotron waves: Waves in multi-ion  
6 magnetosphere, *J. Geophys. Res.*, 111, A10202, doi:10.1029/2006JA011833.  
7
- 8 Khazanov, G. V., K. Gamayunov, D. L. Gallagher, J. U. Kozyra, and M. W. Liemohn (2007) Self-  
9 Consistent Ring Current Modeling with Propagating Electromagnetic Ion Cyclotron Waves in the Presence  
10 of Heavy Ions: 2. Ring Current Ion Precipitation and Wave Induced Thermal Fluxes, *Journal Geophysical  
11 Research*, 112, A04209, doi:10.1029/2006JA012033.  
12
- 13 Khazanov G. V., M. W. Liemohn, T. S. Newman, M.-C. Fok, and A. J. Ridley (2004), Magnetospheric  
14 convection electric field dynamics and stormtime particle energization: case study of the magnetic storm of  
15 4 May 1998, *Annales Geophysicae*, 22: 497-510.  
16
- 17 Lemaire, J. (1985), *Frontiers of the plasmasphere. Thèse d'agrégation de l'Enseignement  
18 Supérieur, Editions Cabay, Louvain-la-Neuve*, ISBN 2-87077-310-2, *Aeronomica Acta A*,  
19 No. 298.  
20
- 21 Lemaire, J. (2000), The Formation of Plasmaspheric Tails. *Phys. Chem. Earth (C)*, 25, 9-17.  
22
- 23 Lemaire, J. F. (2001), The formation of the light-ion trough and peeling off the plasmasphere. *Journal of  
24 Atmospheric and Solar-Terrestrial Physics*, 63, 1285-1291.  
25
- 26 Lemaire, J. F., and K. I. Gringauz, with contributions from D. L. Carpenter and V. Bassolo (1998). *The  
27 Earth's plasmasphere*, Cambridge University Press, Cambridge, 350pp.  
28
- 29 Lemaire J., and L. Kowalkowski (1981), The role of plasma interchange motion for the formation of a  
30 plasmopause, *Planet. Space Sci.*, 29, 4, 469-478.  
31
- 32 Liemohn, M. W., J. U. Kozyra, M. F. Thomsen, J. L. Roeder, G. Lu, J. E. Borovsky, T. E. Cayton (2001),  
33 Dominant role of the asymmetric ring current in producing the stormtime Dst, *Journal of Geophysical  
34 Research*, 106, A6, 10883-10904.  
35
- 36 Liemohn, M. W., A. J. Ridley, D. L. Gallagher, D. M. Ober, J. U. Kozyra (2004), Dependence of  
37 plasmaspheric morphology on the electric field description during the recovery phase of the 17 April 2002  
38 magnetic storm, *Journal of Geophysical Research*, 109, A03209, doi:10.1029/2003JA010304.  
39
- 40 Maynard, N. C., and A. J. Chen (1975), Isolated cold plasma regions: Observations and their relation to  
41 possible production mechanisms, *Journal of Geophysical Research*, 80, 1009-1013.  
42
- 43 McIlwain, C. E. (1986), A Kp dependent equatorial electric field model, *The Physics of Thermal plasma in  
44 the magnetosphere. Advances in Space Research*, 6 (3), pp.187-197.  
45
- 46 Pierrard V. (2006), *The dynamics of the plasmasphere, in Space Science: New Research*", Nova Science  
47 Publishers, Nick S. Maravell Editor, ISBN: 1-60021-005-8.  
48
- 49 Pierrard, V., and J. Lemaire (2004), Development of shoulders and plumes in the frame of the interchange  
50 instability mechanism for plasmopause formation, *Geophysical Research Letters*, 31, 5, L05809,  
51 10.1029/2003GL018919.  
52
- 53 Pierrard, V., and J. Cabrera (2005), Comparisons between EUV/IMAGE observations and numerical  
54 simulations of the plasmopause formation. *Annales Geophysicae*, 23, 7, 2635-2646, SRef-ID: 1432-  
55 0576/ag/2005-23-2635.  
56

- 1 Pierrard, V., and J. Cabrera (2006), Dynamical simulations of plasmopause deformations, *Space Science*  
2 *Reviews (WSEF)*, 122, Issue 1-4, 119-126, doi: 10.1007/s11214-005-5670-8.
- 3
- 4 Rasmussen C. E. (1992), The plasmasphere, *Physics of Space Plasmas (1992)*, eds: Chang T. and J. R.  
5 Jasperse, Scientific Publishers, Inc. Cambridge, Massachusetts, 279-302.
- 6
- 7 Richmond, A. D., and Y. Kamide (1988), Mapping electrodynamic features of the high-latitude ionosphere  
8 from localized observations: Technique, *J. Geophys. Res.*, 93, 5741-59.
- 9
- 10 Spasojevic M., H. U. Frey, M. F. Thomsen, S. A. Fuselier, S. P. Gary, B. R. Sandel, U. S. Inan (2004), The  
11 link between a detached subauroral protons arcs and a plasmaspheric plume, *Journal Geophysical*  
12 *Research*, 112, A04209, doi:10.1029/2006JA012033.
- 13
- 14 Stern, D. P. (1975), The motion of a proton in the equatorial magnetosphere. *Journal of Geophysical*  
15 *Research*, 80, 595.
- 16
- 17 Summers, D. and R. M. Thorne (2003), Relativistic Electron Pitch-Angle Scattering by Electromagnetic  
18 Ion Cyclotron Waves During geomagnetic Storms, *J. Geophys. Res.*, 108, NO. A4,  
19 10.1029/2002JA009489.
- 20
- 21 Tsyganenko, N. A. (1996), Modeling the global magnetic field of the large-scale Birkeland current systems,  
22 *J. Geophys. Res.*, 101, 27, 187.
- 23
- 24 Volland, H. (1973), A semiempirical model of large-scale magnetospheric electric fields, *Journal of*  
25 *Geophysical Research*, 78, 171-180.
- 26
- 27 Weimer, D. R. (1996), A flexible, IMF dependent model of high-latitude electric potentials having "space  
28 weather" applications, *Geophys. Res. Lett.*, 23, 18, 1549-2552.
- 29
- 30
- 31

## 32 Figure captions

33

34 Figure 1: Equipotential contours of the Kp-dependent convection electric field Volland-  
35 Stern on 28 October 2001 (without co-rotation electric field).

36

37 Fig. 2: Equipotential map of the Kp-dependent convection electric field E5D on 28  
38 October 2001 (without co-rotation electric field).

39

40 Fig. 3: Magnetic field model M2.

41

42 Fig. 4: Equipotential map of the Weimer convection electric field dependent on solar  
43 wind conditions on 28 October 2001 (without co-rotation electric field).

44

45 Fig. 5: Equipotential map of the total electric field Volland-Stern on 28 October 2001.  
46 Same as Fig. 1 but with co-rotation.

47

48 Fig. 6: Equipotential map of the total electric field E5D on 28 October 2001. Same as  
49 Fig. 2 but with co-rotation.

50

51 Fig. 7: Equipotential map of the Weimer total electric field dependent on 28 October  
52 2001. Same as Fig. 4 but with co-rotation.

1  
2 Fig. 8: Variation of the solar wind density of protons, the solar wind velocity and the Bx  
3 and By component of the magnetic field.  
4

5  
6 Fig. 9: Initial plasmasphere determined with the MHD simulations using the E5D E-field  
7 model (upper left panel), MHD with Volland-Stern model (upper middle panel), MHD  
8 with Weimer model (upper right panel) and the plasmopause position predicted by  
9 instability mechanism with E5D (bottom left panel) on 28 October 2001 at 0:00 UT. All  
10 these simulations started at 0:00 UT, 27 October 2001. The upper panels show the values  
11 of the Northward component of the interplanetary magnetic field (Bz), the value of the  
12 ring current magnetic field (Dst in nT), and the values of the geomagnetic index Kp  
13 during 3 days between 27 October 2001 and the end of 29 October 2001. No observations  
14 from EUV/IMAGE are available at that time.  
15

16 Fig. 10: Results of the MHD E5D simulations (upper left panel), MHD VSMC (upper  
17 middle panel), MHD W (upper right panel), IC E5D (bottom left panel) at 4:30 UT, 28  
18 October 2001. The EUV/IMAGE observation of the equatorial plasmopause position at  
19 4:39 UT is illustrated in the bottom right panel.  
20

21 Fig. 11: Results of the MHD E5D simulation (upper left panel), MHD VSMC (upper  
22 middle panel), MHD W (upper right panel), IC E5D (bottom left panel) at 8:00 UT, 28  
23 October 2001. The EUV/IMAGE observation of the equatorial plasmopause position at  
24 8:03 UT is illustrated in the bottom right panel.  
25

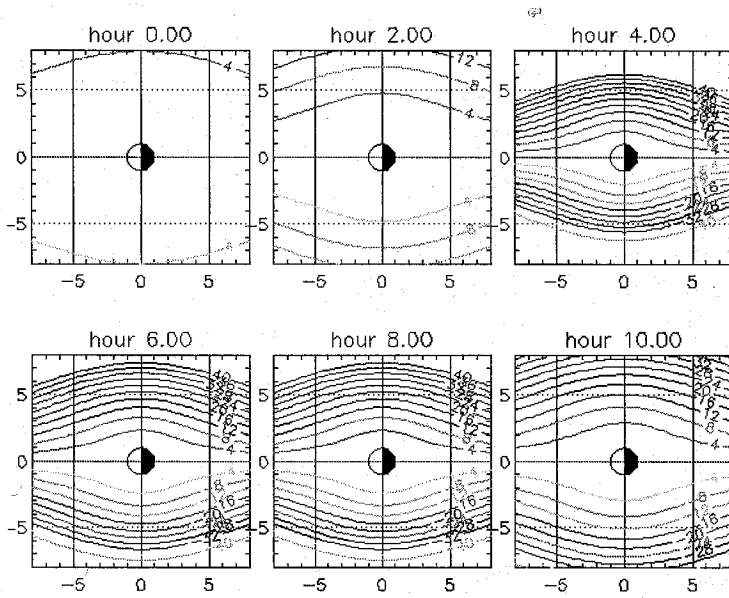
26 Fig. 12: Results of the MHD E5D simulation (upper left panel), MHD VSMC (upper  
27 middle panel), MHD W (upper right panel), IC E5D (bottom panel) at 12:00 UT, 28  
28 October 2001. No EUV/IMAGE observation is available at that time.  
29

30 Fig.13: Results of the MHD E5D simulation (upper left panel), MHD VSMC (upper  
31 middle panel), MHD W (upper right panel), IC E5D (bottom left panel) at 18:00 UT, 28  
32 October 2001. The EUV/IMAGE observation of the equatorial plasmopause position at  
33 18:05 UT is illustrated in the bottom right panel.  
34

35 Fig. 14: Results of MHD E5D simulations (upper left panel), MHD VSMC (upper middle  
36 panel), MHD W (upper right panel), IC E5D (bottom left panel) at 20:00 UT, 28 October  
37 2001. The EUV/IMAGE observation of the equatorial plasmopause position at 19:58 UT  
38 is illustrated in the bottom right panel.  
39

40 Figure 15: Results of MHD E5D simulations (upper left panel), MHD VSMC (upper  
41 middle panel), MHD W (upper right panel), IC E5D (bottom left panel) at 21:00 UT,  
42 after the magnetic storm of 17 April 2002. The EUV/IMAGE observation of the  
43 equatorial plasmopause position at 21:07 UT is illustrated in the bottom right panel.  
44  
45  
46  
47

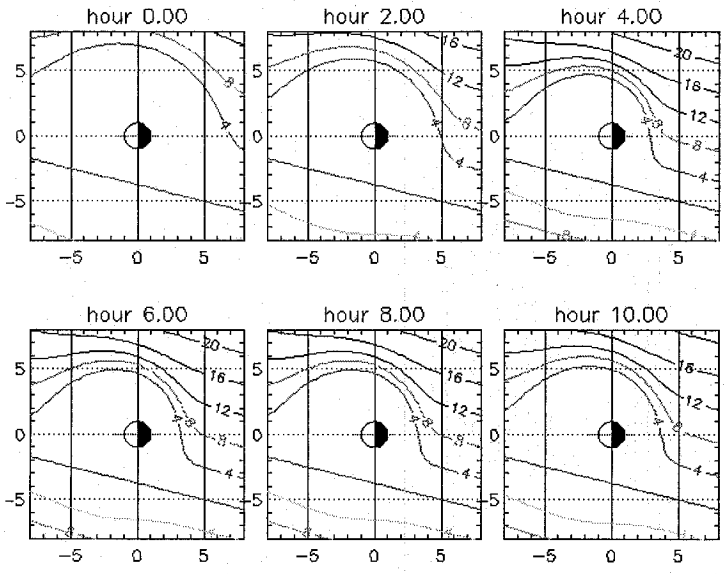
1 Figure 1: Equipotential contours of the Kp-dependent convection electric field Volland-  
2 Stern on 28 October 2001 (without co-rotation electric field).  
3  
4  
5



6  
7  
8  
9  
10  
11  
12  
13  
14  
15  
16  
17  
18  
19  
20  
21  
22  
23  
24  
25  
26  
27  
28  
29  
30

1  
2  
3  
4  
5  
6  
7

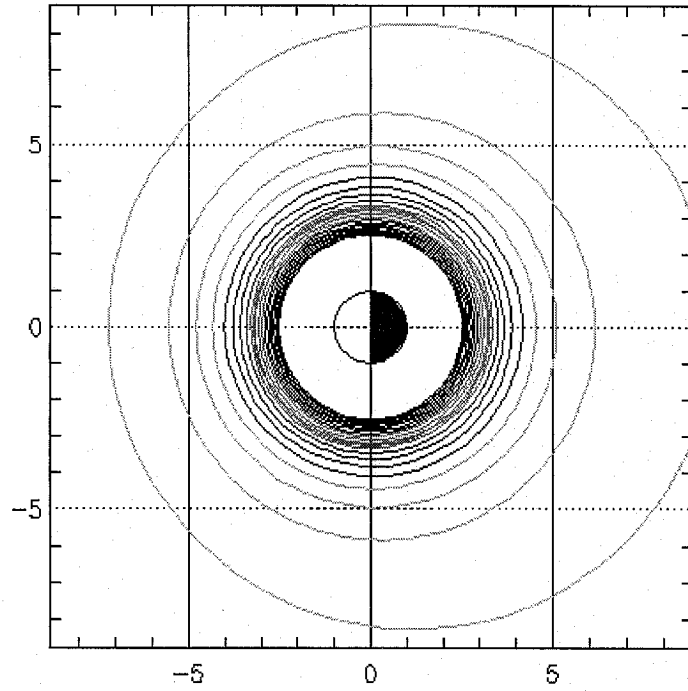
Fig. 2: Equipotential map of the Kp-dependent convection electric field E5D on 28 October 2001 (without co-rotation electric field).



8  
9  
10  
11  
12  
13  
14  
15  
16  
17  
18  
19  
20  
21  
22  
23  
24  
25  
26  
27  
28  
29  
30  
31

1  
2  
3

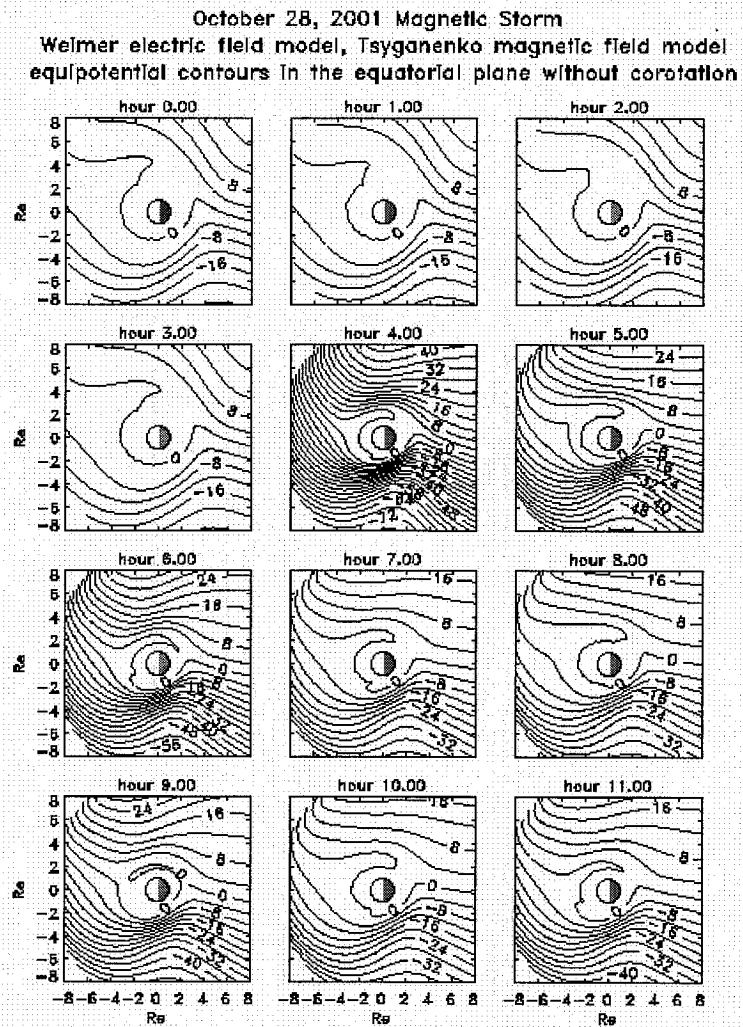
Fig. 3: Magnetic field model M2.



4  
5  
6  
7  
8  
9  
10  
11  
12  
13  
14  
15  
16  
17  
18  
19  
20



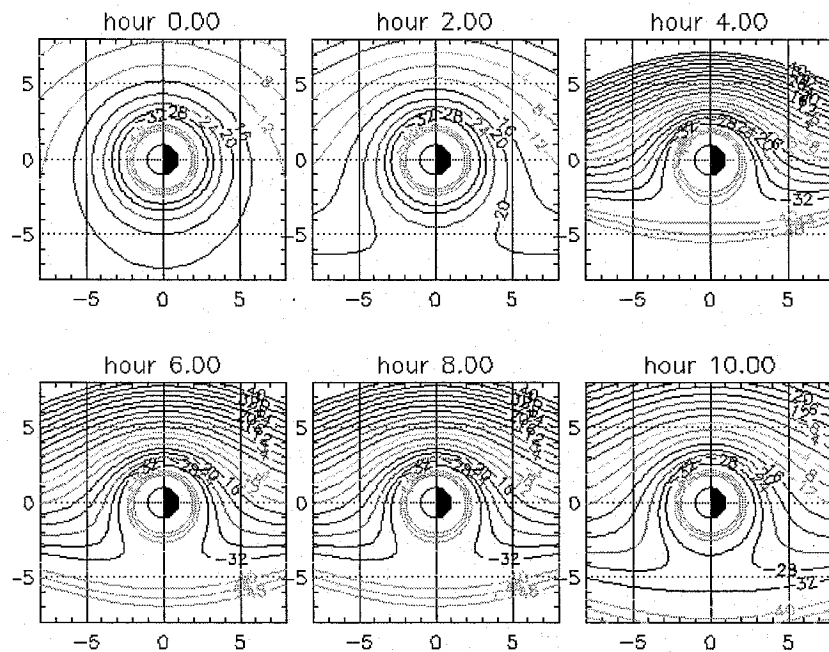
- 1 Fig. 4: Equipotential map of the Weimer convection electric field dependent on solar
- 2 wind conditions on 28 October 2001 (without co-rotation electric field).



3

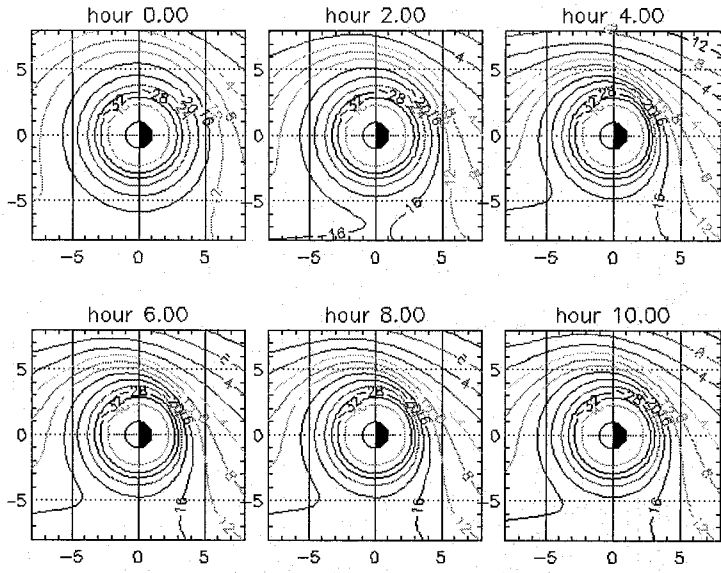
1  
2  
3  
4  
5  
6

Fig. 5: Equipotential map of the total electric field Volland-Stern on 28 October 2001.  
Same as Fig. 1 but with co-rotation.



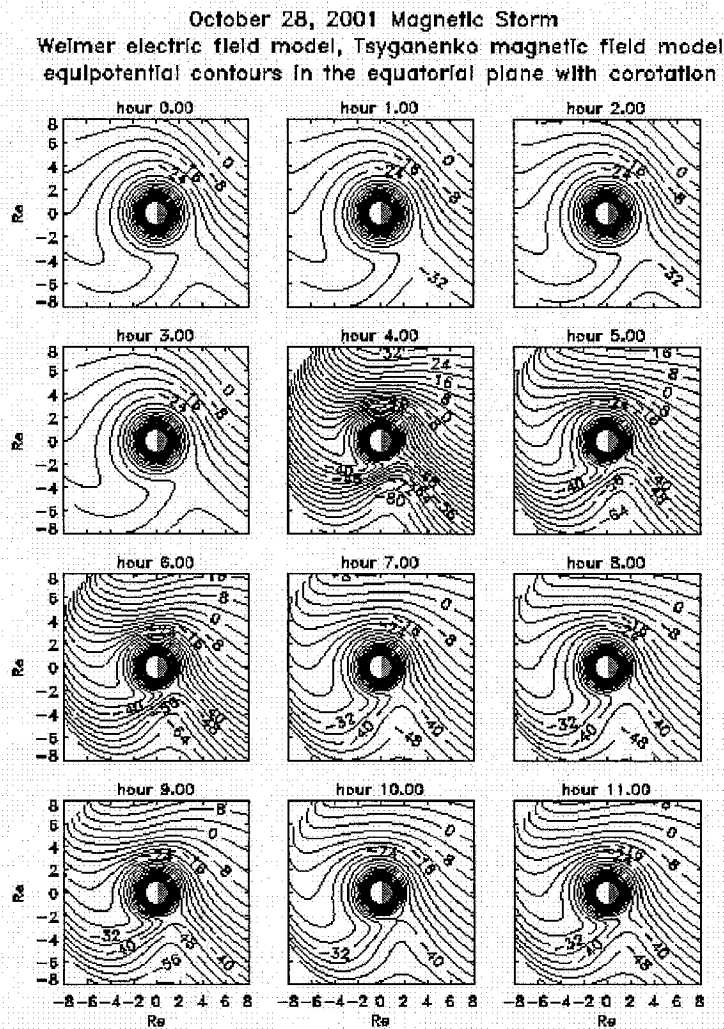
7  
8  
9  
10  
11  
12  
13  
14  
15  
16  
17  
18  
19  
20  
21  
22  
23  
24  
25  
26  
27

1 Fig. 6: Equipotential map of the total electric field E5D on 28 October 2001. Same as  
2 Fig. 2 but with co-rotation.  
3  
4



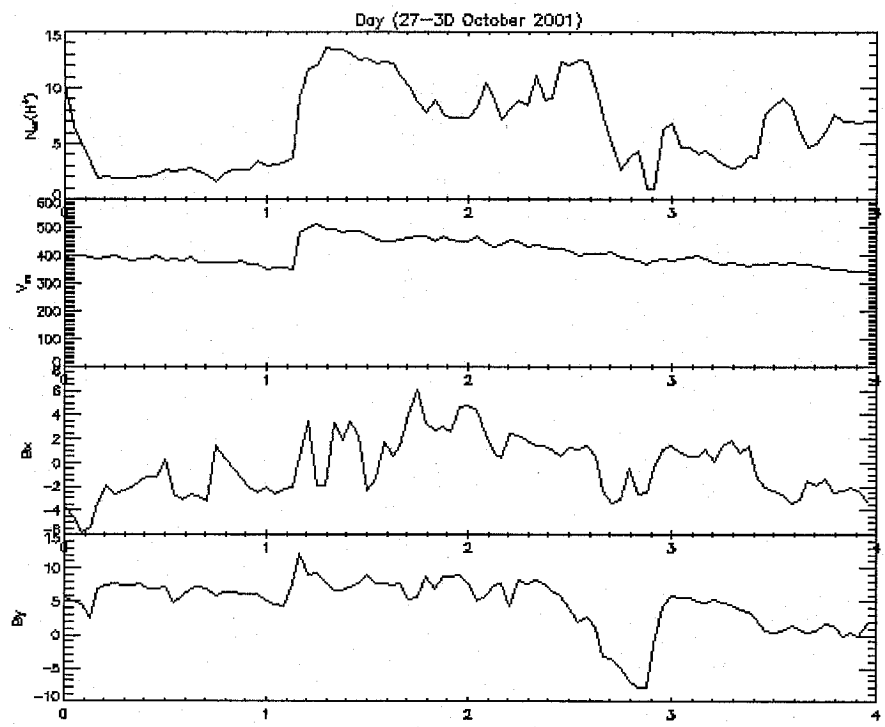
- 5
- 6
- 7
- 8
- 9
- 10
- 11
- 12
- 13
- 14
- 15
- 16
- 17
- 18
- 19
- 20
- 21
- 22
- 23
- 24
- 25
- 26
- 27
- 28
- 29
- 30
- 31

- 1 Fig. 7: Equipotential map of the Weimer total electric field dependent on 28 October
- 2 2001. Same as Fig. 4 but with co-rotation.



1  
2  
3  
4  
5  
6  
7  
8  
9  
10  
11  
12  
13  
14

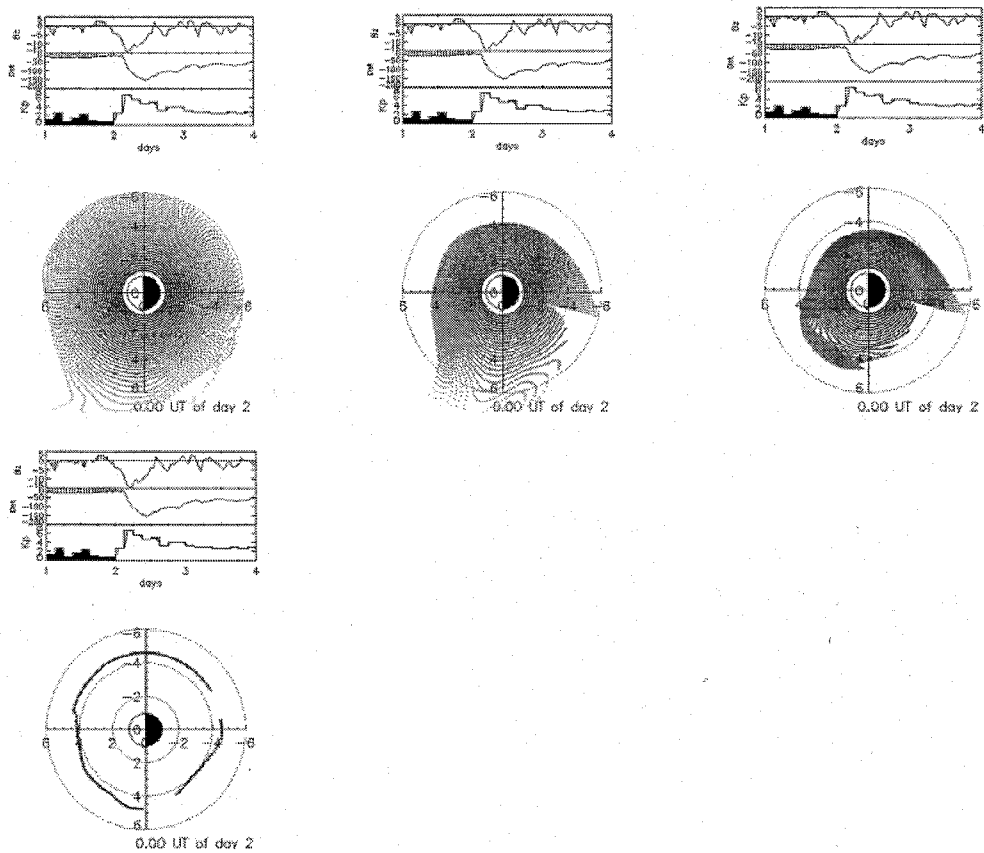
Fig. 8: Variation of the solar wind density of protons, the solar wind velocity and the Bx and By component of the magnetic field.



15  
16  
17  
18  
19  
20  
21  
22  
23  
24

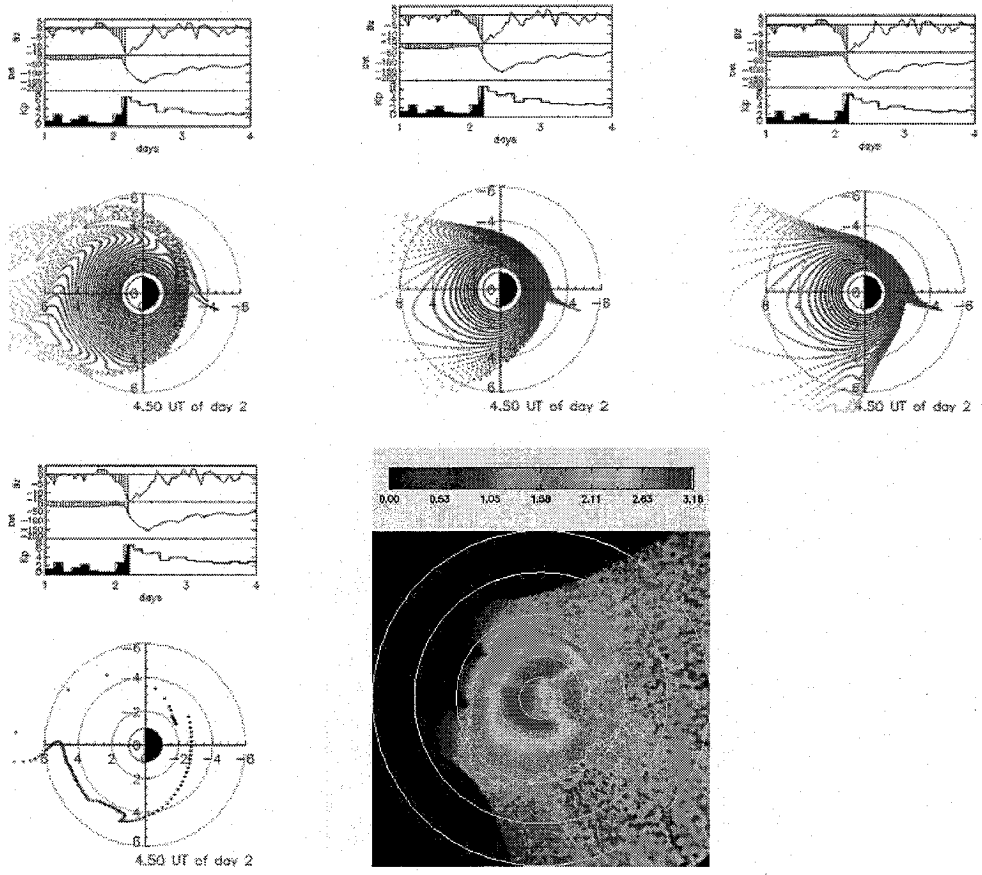
1  
2  
3  
4  
5  
6  
7  
8  
9  
10  
11

Fig. 9: Initial plasmasphere determined with the MHD simulations using the E5D E-field model (upper left panel), MHD with Volland-Stern model (upper middle panel), MHD with Weimer model (upper right panel) and the plasmapause position predicted by instability mechanism with E5D (bottom left panel) on 28 October 2001 at 0:00 UT. All these simulations started at 0:00 UT, 27 October 2001. The upper panels show the values of the Northward component of the interplanetary magnetic field ( $B_z$ ), the value of the ring current magnetic field (Dst in nT), and the values of the geomagnetic index  $K_p$  during 3 days between 27 October 2001 and the end of 29 October 2001. No observations from EUV/IMAGE are available at that time.



1  
2  
3  
4  
5  
6  
7

Fig. 10: Results of the MHD E5D simulations (upper left panel), MHD VSMC (upper middle panel), MHD W (upper right panel), IC E5D (bottom left panel) at 4:30 UT, 28 October 2001. The EUV/IMAGE observation of the equatorial plasmapause position at 4:39 UT is illustrated in the bottom right panel.

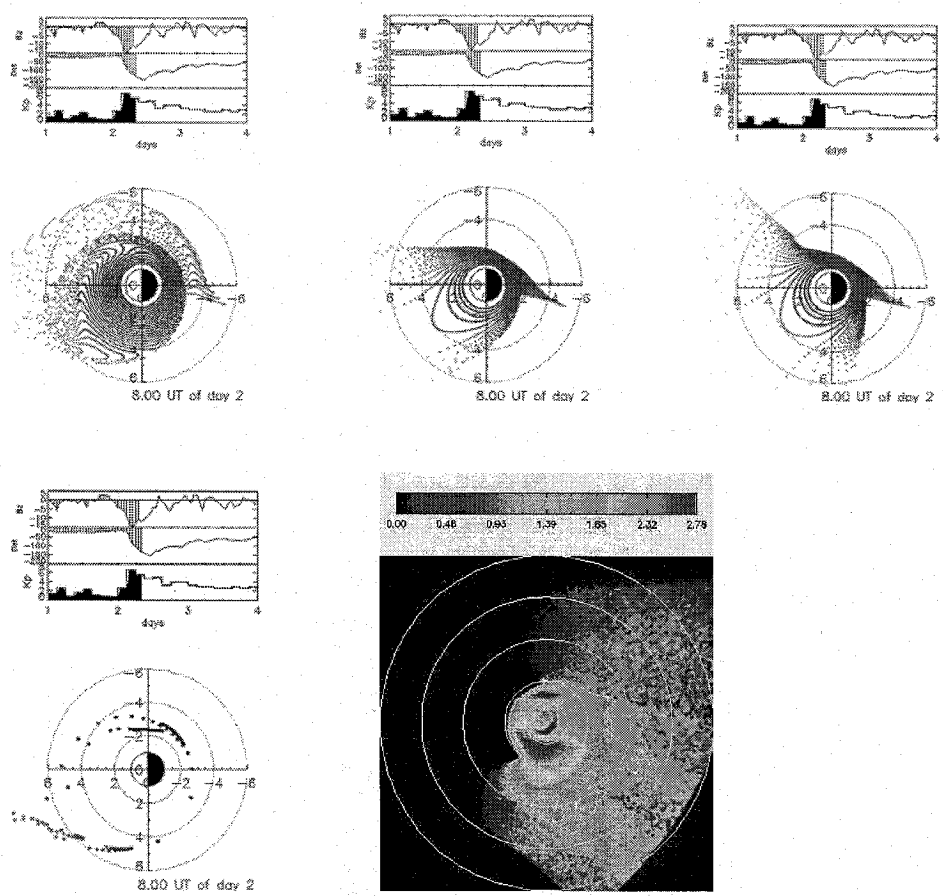


8  
9

10  
11  
12  
13  
14  
15  
16  
17  
18  
19  
20  
21  
22  
23  
24  
25

1  
2  
3  
4  
5  
6

Fig. 11: Results of the MHD E5D simulation (upper left panel), MHD VSMC (upper middle panel), MHD W (upper right panel), IC E5D (bottom left panel) at 8:00 UT, 28 October 2001. The EUV/IMAGE observation of the equatorial plasmopause position at 8:03 UT is illustrated in the bottom right panel.



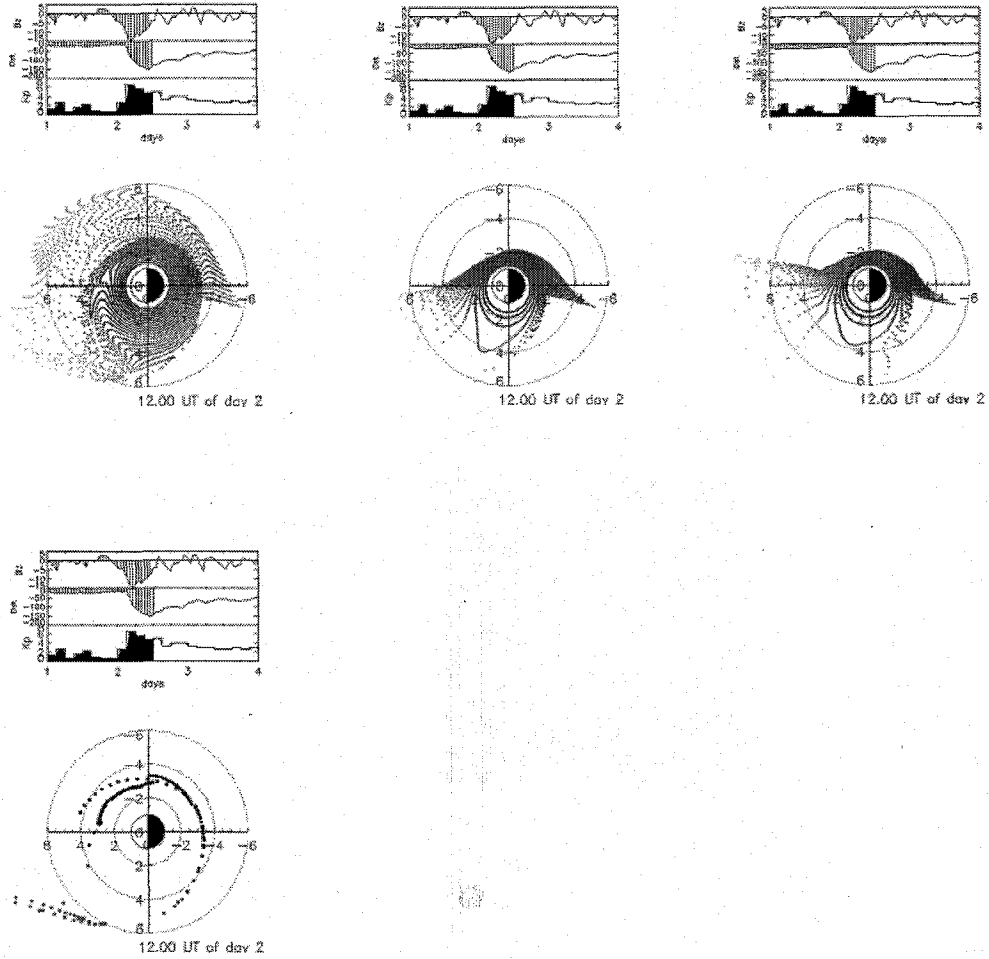
7  
8  
9

10  
11  
12  
13  
14  
15  
16  
17  
18  
19  
20  
21  
22  
23  
24  
25



1  
2  
3  
4  
5  
6

Fig. 12: Results of the MHD E5D simulation (upper left panel), MHD VSMC (upper middle panel), MHD W (upper right panel), IC E5D (bottom panel) at 12:00 UT, 28 October 2001. No EUV/IMAGE observation is available at that time.

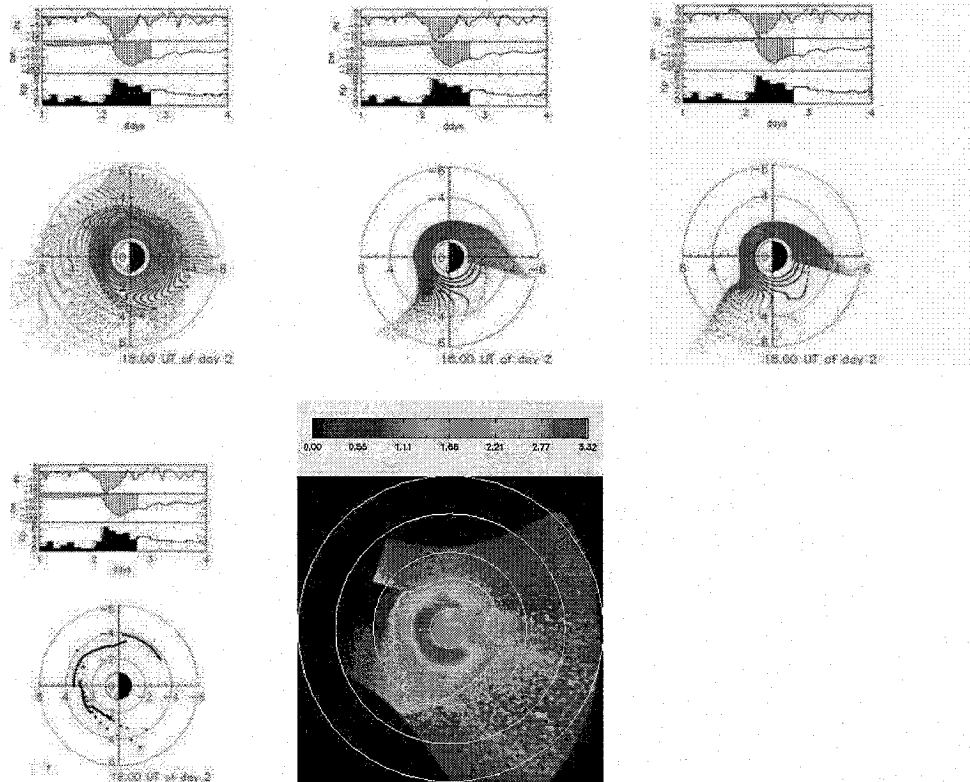


7  
8  
9  
10  
11

12  
13  
14  
15  
16  
17  
18  
19  
20  
21  
22  
23  
24  
25

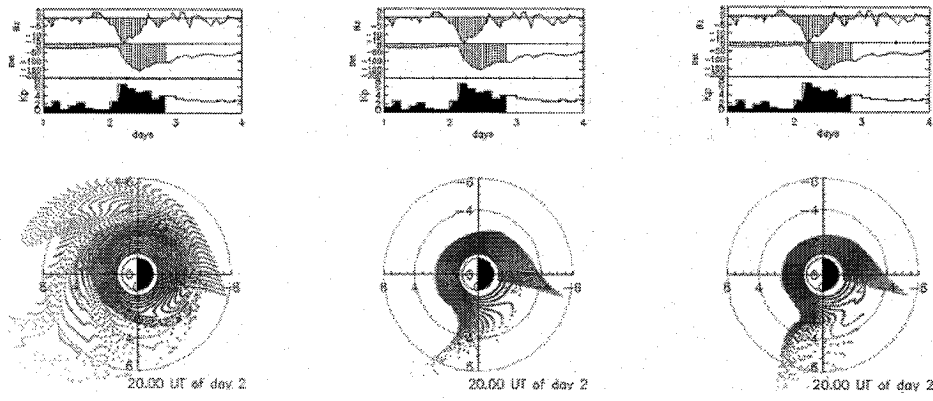
1  
2  
3  
4  
5  
6  
7  
8  
9  
10  
11  
12  
13  
14  
15  
16  
17  
18  
19  
20  
21  
22  
23  
24  
25  
26  
27

Fig.13: Results of the MHD E5D simulation (upper left panel), MHD VSMC (upper middle panel), MHD W (upper right panel), IC E5D (bottom left panel) at 18:00 UT, 28 October 2001. The EUV/IMAGE observation of the equatorial plasmopause position at 18:05 UT is illustrated in the bottom right panel.

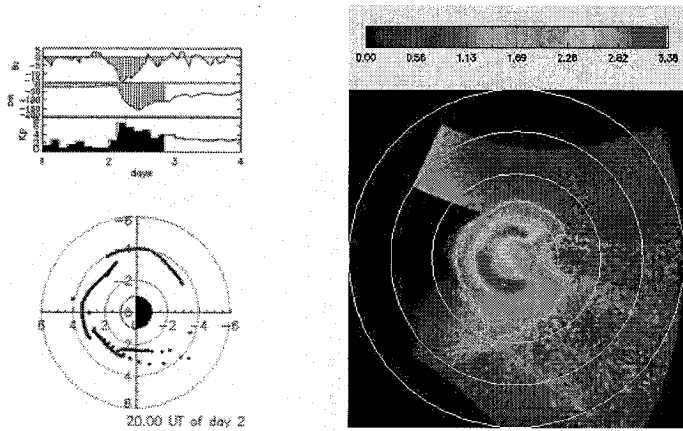


1 Fig. 14: Results of MHD E5D simulations (upper left panel), MHD VSMC (upper middle  
 2 panel), MHD W (upper right panel), IC E5D (bottom left panel) at 20:00 UT, 28 October  
 3 2001. The EUV/IMAGE observation of the equatorial plasmopause position at 19:58 UT  
 4 is illustrated in the bottom right panel.

5



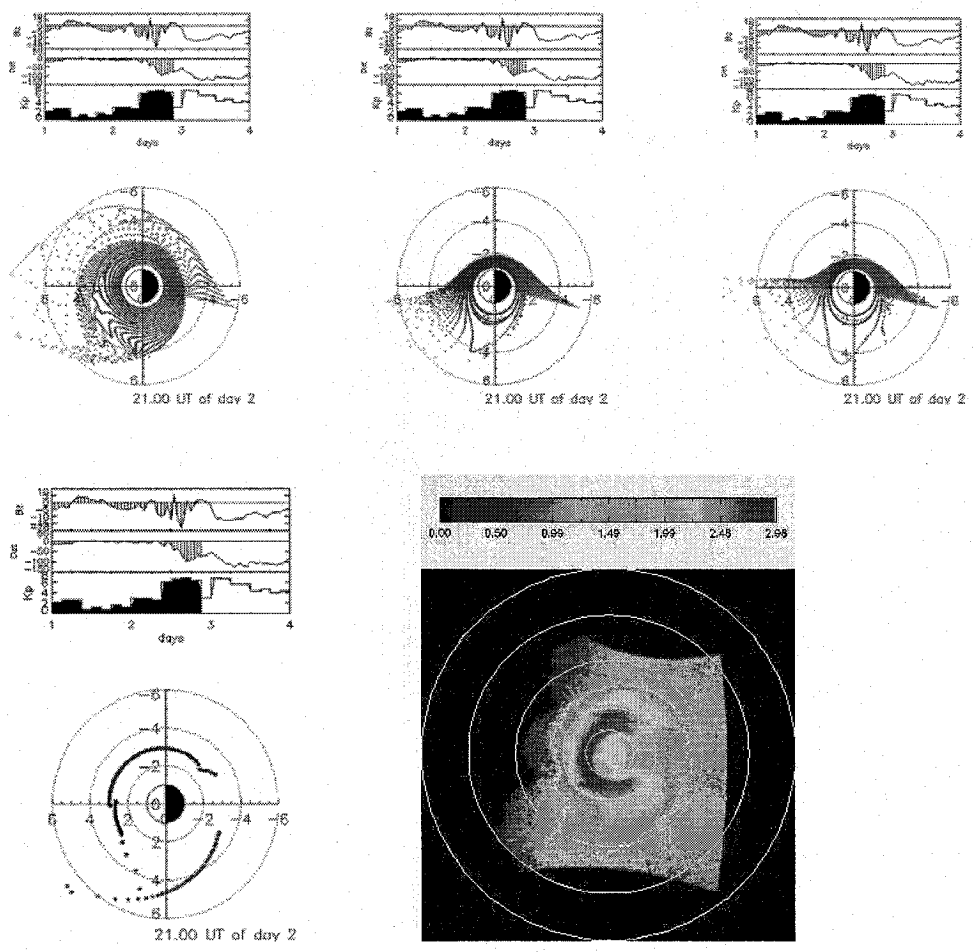
6  
7



8  
9  
10  
11  
12  
13  
14  
15  
16  
17  
18  
19  
20  
21  
22  
23  
24  
25  
26

1  
2  
3  
4  
5  
6  
7  
8  
9  
10  
11  
12  
13  
14

Figure 15: Results of MHD E5D simulations (upper left panel), MHD VSMC (upper middle panel), MHD W (upper right panel), IC E5D (bottom left panel) at 21:00 UT, after the magnetic storm of 17 April 2002. The EUV/IMAGE observation of the equatorial plasmapause position at 21:07 UT is illustrated in the bottom right panel.



15  
16  
17

18  
19  
20  
21  
22  
23